Ultrasonics Sonochemistry 89 (2022) 106151

Contents lists available at ScienceDirect

Ultrasonics Sonochemistry

journal homepage: www.elsevier.com/locate/ultson

An overview and critical assessment of the mechanisms of microstructural refinement during ultrasonic solidification of metals

Nagasivamuni Balasubramani, Jeffrey Venezuela, Nan Yang, Gui Wang, David StJohn, Matthew Dargusch *

Centre for Advanced Materials Processing and Manufacturing (AMPAM), School of Mechanical and Mining Engineering, University of Queensland, St Lucia, QLD 4072, Australia

ARTICLE INFO

Keywords:
Ultrasonic treatment
Grain refinement
Intermetallic refinement
Solidification
Light metals
Zinc alloys

ABSTRACT

A refined, equiaxed grain structure and the formation of finer primary intermetallic phases are some of the notable benefits of ultrasonic processing of liquid/solidifying melts. Ultrasonic treatment (UST) has been widely explored in Al and Mg-based alloys due to its operational versatility and scalability. During UST, the refinement of grain and primary intermetallic phases occurs via cavitation-induced fragmentation mechanisms. In addition, UST improves the efficiency (activation of particles) of the conventional grain refinement process when potent particles are added through master alloys. Though the UST's ability to produce refined as-cast structures is well recognized, the understanding of the refinement mechanisms is still debated and unresolved. Significant efforts have been devoted to understanding these mechanisms through the use of sophisticated techniques such as in-situ/ real-time observation, lab-scale and commercial-scale casting processes. All these studies aim to demonstrate the significance of cavitation, fragmentation modes, and alloy chemistry in microstructure refinement. Although the physical effects of cavitation and acoustic streaming (fluid flow) are primary factors influencing the refinement, the dominant grain refinement mechanisms are affected by several solidification variables and casting conditions. Some of these include melt volume, solute, cooling rate, potent particles, grain growth (equiaxed, columnar or dendritic), and the cold zones of the casting where the onset of nucleation occurs. This review aims to provide a better insight into solidification variables emphasizing the importance of cold zones in generating fine structures for small- and large-volume (direct chill) castings. Another important highlight of this review is to present the relatively less explored mechanism of (acoustic) vibration-induced crystallization and discuss the role of cavitation in achieving a refined ingot structure.

1. Introduction

Refinement of microstructural constituents is imperative in forming the solidification structure regardless of the volume of the metal solidified (e.g., as seen in processes such as soldering, welding, additive manufacturing, permanent mould casting and direct chill casting) [1–4]. In cast alloys, the refinement of a particular phase or grains is promoted by the addition of chemical modifiers (Sr/AlP addition for Si phase [5]) or a master alloy containing potent nucleation particles (e.g. Al-Ti-B master alloy) [2,3]. Although some refiners are commercially established and widely used in foundries, developing an understanding of the grain refinement mechanism and the interaction of impurity elements or any other alloying elements that influences process efficiency are the most investigated research topics in solidification processing by chemistry modification [6–8].

Fig. 1 presents a broad overview of the research progress in the solidification field for the keywords "solidification" and "grain refinement". The results are carefully filtered using enhanced keyword search criteria. Refinement of microstructural constituents to achieve a better mechanical property is an active area in various streams of solidification research (casting, welding and additive manufacturing). One of the key aspects of external field processing of liquid/solidifying metal is that the refinement is unrestricted by the alloy chemistry and brings significant reduction to the primary intermetallic phases and grain structures [9,10]. The keyword search for prominent external field techniques such as "ultrasonic" and "magnetic" fields together revealed a significant contribution to solidification processing (~35 % of total articles). Studies in ultrasonic processing gained considerable interest due to the

* Corresponding author.
E-mail address: m.dargusch@uq.edu.au (M. Dargusch).

https://doi.org/10.1016/j.ultsonch.2022.106151
Received 22 June 2022; Received in revised form 23 August 2022; Accepted 28 August 2022
Available online 30 August 2022

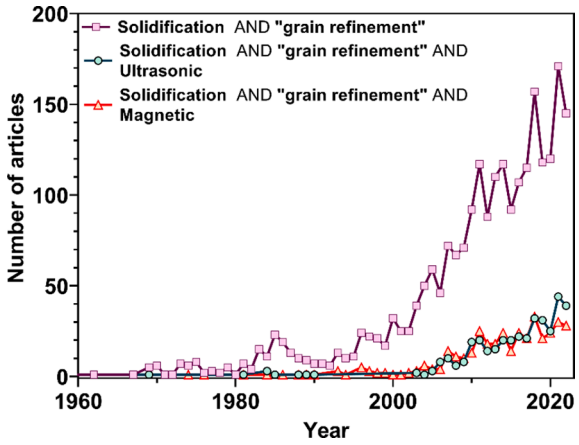

Fig. 1. Literature survey showing the number of publications that appeared in the Scopus search for the keywords "Solidification", "grain refinement", "ultrasonic" and "magnetic" fields. The broad search results were further refined by limiting unrelated keywords or topics.

versatility of application to Al alloy's casting and degassing process [11,12]. Significant interest has grown in the last decade due to the application of ultrasonics in emerging fields like additive manufacturing [13–15]. In casting and solidification, contributions by O.V. Abramov [16,17] and G. I. Eskin [10,18] to the fundamentals of UST and the commercial importance of applying UST to direct chill (DC) cast ingots and degassing processes in Al alloys are notable. Several research works published later on include lab-scale experiments that investigated (but are not limited to) the role of solute [19–21] and nucleant particles on grain refinement [22,23], refinement of primary intermetallic phases [20,21,24], solidification of immiscible systems [25], degasification [26], development of metal matrix nano-composites [27], simulating the effect of temperature gradient and fluid flow affecting the solidification structure [28–31]. Transparent analogues [32–35] and water models [36,37] were used to understand the cavitation phenomenon, which progressed significantly with further advancement in in-situ characterization using X-ray synchrotron imaging techniques [38–42].

Fig. 2(a) shows a photograph of the UST applied to Al-2.0 wt%Cu alloy in a typical lab-scale experiment, while Fig. 2 (b and c) present the macrostructures before and after UST [43]. It is interesting to note that the grain refinement after UST is uniform throughout the ingot, and identifying the mechanism responsible for such refinement is one of the most debated and controversial research subjects. Fig. 2(d) shows the classification of mechanisms reported for UST and other external field methods. For UST, the commonly cited mechanisms include the enhancement of nucleation and fragmentation of dendrites due to cavitation and acoustic streaming. In most of the alloys examined after UST (shown in Fig. 2(c)), the refined grains are non-dendritic and much finer than the secondary dendritic arm spacing of the as-cast alloy. Due to the spherical morphology and uniform distribution of the grains after UST, earlier studies supported a nucleation-based mechanism for grain refinement [44]. A pressure pulse mechanism (large undercooling generated after bubble implosion) preferentially enabling nucleation on impurity or oxide particles was proposed for the refinement shown in Fig. 2(d) [12,44–46]. This idea was borrowed from high-pressure solidification techniques. Here, the application of high pressure causes a shift in equilibrium temperatures resulting in a large undercooling and subsequently enhancing the nucleation of grains [47]. Secondly, the nucleation mechanism is supported by studies that involve mechanical stirring or semisolid processing methods whenever non-dendritic,

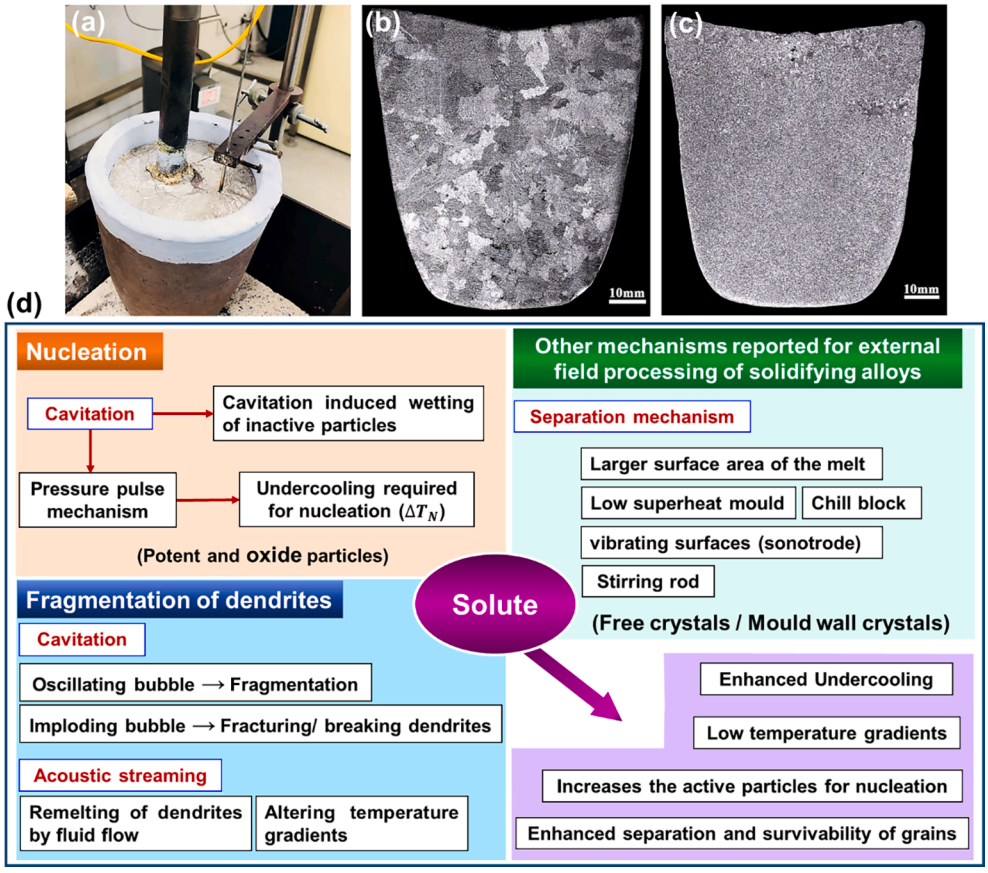

Fig. 2. (a) Photograph of UST applied during the solidification of Al-2.0wt%Cu alloy. Macrostructures showing the grain structure before (b) and after UST (c) [43]. (d) A schematic outline of the classification of mechanisms reported for ultrasonic processing, other external field techniques and the role of solute.

spherical grains are noted (usually under high stirring speeds) [48–50]. This nucleation is likely due to the activation of non-wettable oxide particles as a result of intense convection and low temperature gradients.

The concept of dendritic fragmentation through shearing and remelting of secondary dendritic arms was also adopted from the semisolid processing techniques [51,52]. However, the visualisation of cavitation bubbles becomes possible in metallic melts with the help of the in-situ techniques that advanced the understanding and established the roles of cavitation bubbles and acoustic streaming in the fragmentation of solid phases [38–41]. The dynamic life of oscillating and imploding cavitation bubbles, the role of streaming flow enabling fragmentation and the distribution of fragmented phases are evident in these investigations [40]. Thus, it is generally agreed that cavitation and fluid flow-associated (e.g. by acoustic streaming) fragmentation is responsible for the refinement observed after UST.

Recent research by the authors indicated that many disputes exist on the mechanism of grain refinement within the external field processing of solidifying alloys (e.g. ultrasonic, magnetic, electric and mechanical stirring methods) [53,54]. Currently, no mechanism is universally accepted or explains refinement in the recognized technique (for instance, stirring, electric or magnetic field solidification techniques) [54,55]. Researchers also recognized that the dominant mechanism (either nucleation and/or fragmentation) could shift as influenced by changes in solidification conditions (conventional, directional, or in-situ methods) [53]. In the case of UST, the refinement mechanism is often associated with cavitation and fluid flow caused by acoustic streaming. However, one of the most underexplored mechanisms is the formation of fine grains due to an applied high-frequency vibration during solidification [54–56].

The frequencies of mechanical vibration techniques can range from as low as 20 Hz up to 10 kHz [57]. Usually, vibrations are applied through the mould wall (through the vibrating table) [58] or by direct irradiation. These vibrations induce refinement by ejecting fine crystals from the vibrated rod (regions surrounding the vibrator) [59] or detaching dendrites from the mould wall and melt surface [12,53,54,57]. The effect of vibrating frequency, amplitude and temperature range of solidification was studied to produce the finest grain structure in the ingot and also to understand the mechanisms of refinement [60]. In contrast, ultrasonic vibrations have lower amplitude and frequencies over 16 kHz, which is powerful enough to create unique (capillary) wave patterns and cavitation at the bottom surface of the sonotrode [61–63]. This principle is largely explored in ultrasonic atomizers to produce fine liquid droplets or liquid metals to produce powder particles [64,65].

Solidification research in UST has not explored the role of ultrasonic vibration effects in generating fine grains and their contribution to the overall grain refinement [56]. Therefore, the main objective of this review is to explore and highlight the formation of fine grains through high-frequency vibrations during UST. In order to explain this mechanism, the first section presents a brief review emphasizing the role of solute and potent nucleation particles. The attributes of the role of solute and potent particles contributing to the UST refinement are well-known and are shown in Fig. 2(d) [53,54]. Secondly, this review discusses the role of cavitation in producing fine grains. Some pertinent questions to address are ‘does the formation of fine grains require the occurrence of cavitation and implosion of bubbles?’ and ‘what is the role of acoustic streaming?’. A comparative study of cooling rate vs cavitation-induced fragmentation is examined in Zn-based alloys for the refinement of the primary $CaZn_{13}$ intermetallic phase in Zn-Ca-Cu alloys [66].

The final section of this paper critically compares the refinement and the mechanism that promotes grain refinement in lab-scale conditions vs the direct chill (DC) casting process that employs UST in large-scale castings [30,31,67]. The importance of cold zones in the casting and how the onset of solidification near the relatively cold zones can produce finer grains when separated by vibration or agitations will also be discussed [54,55,68].

The reader should be aware that, in this review, fragmentation refers to the new solid phases/fragments created from the already solidified/solidifying grain or primary intermetallic phase. For the grains originating from the mould wall or vibrating surface, the term separation (coined by Ohno [69,70]) was used because such crystal multiplication is different from the fragmentation of a dendrite or nucleation from the suspended heterogeneous particles within the melt.

Recently published review articles have summarized the effects of UST during in-situ solidification [9] and in conventional solidification for the origin of fine grains (including other external field methods) [43,54]. Therefore, such mechanisms or ideas will not be repeated here for brevity. However, some results are reproduced or discussed here briefly to provide adequate background for the mechanistic viewpoints highlighted in this review along with a few additional experiments.

2. Ultrasonic processing conditions, alloy systems and solidification variables

Fig. 3 shows the outline of some of the prominent alloy systems and solidification variables reviewed for grain refinement and primary intermetallic phases. Solute and potent particles are important contributing factors to grain refinement. Pure metals can be generally characterized to have unknown nucleant particles (oxides or other impurities) and an inadequate amount of solute. Solute addition in eutectic or peritectic alloys promotes refinement, which is explained by a growth restriction factor (GRF$= mC_0(k-1)$, where m is the slope of the liquidus line and k is the partition coefficient for solute content $C_0 = 1.0wt.\%$)), Generally, higher GRF of solute and potent particles added through grain refining master alloy constitute a better refinement [8,71]. Disputes still exist regarding the mechanisms based on circumstantial evidence specific to the casting condition and alloy composition. For instance, in pure metals and eutectic alloys (e.g., Mg-Al, Mg, Zn, Al-Cu and Al-Si alloys), the formation of non-dendritic grains is supported by the activation of oxide or impurity particles (by a pressure-pulse mechanism [12,44–46]), while in peritectic alloys (Mg-Zr [72] and Al-Ti or Al-Cu-Ti alloys [43]) the UST refinement is attributed to the enhancement of nucleation on potent particles. Fragmentation of dendrites by cavitation or fluid flow is endorsed in both these cases as an additional mechanism. Few alloys solidify with a large fraction of primary intermetallic phases (mainly Al alloys used in non-structural components compared to Mg alloys) in which the dominant mechanism for refinement is fragmentation by cavitation and fluid flow, although some oxide particles are found as nucleating substrates after UST [43,73]. The refinement induced by cavitation and acoustic streaming (for a given volume of melt) is dependent on the intensity of the applied power of UST [74]. However, for the separation mechanisms listed in Fig. 2(d), several additional factors could play a dominant role in generating fine grains. Some of these include the temperature of the mould (promoting mould wall nucleation), vibrations or stirring applied on the surface of the melt, sonotrode preheat temperature and cooling rate, as shown in Fig. 3 [53–55]. Finer grains generated by acoustic vibration effects are often misrepresented as the grains formed due to nucleation or fragmentation effects. Similarly, the cooling rate, UST temperature range of application, and mould wall nucleation can affect the dominant mechanism for the refinement of primary intermetallic phases. All the listed solidification variables in Fig. 3 are separately discussed in the respective sections in detail for grain refinement and primary intermetallic refinement. Since the role of solute and nucleation particles are widely reported and discussed in Al-based alloys [19–21,75–77] and Mg-based alloys [72,78–80], this review explores the application of UST to Zn-based alloys [66,81,82].

Some additional experiments performed in Zn-based alloys are listed in Table 1. Zn-Al alloys are initially melted using high purity ingots in the induction melting furnace (for nearly 3 kg) at an operating power of 8 kW and remelted in an electrical resistance melting for UST in a

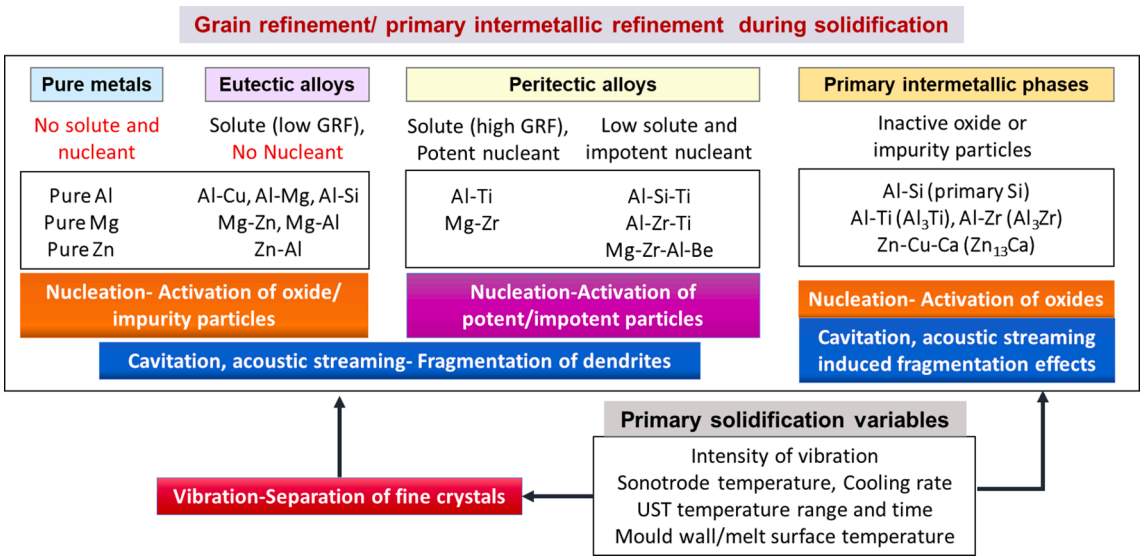

Fig. 3. Pure metals, alloy systems and solidification variables reviewed for the key mechanisms influencing grain and primary intermetallic refinement.

Table 1
UST of Zn-Al and Zn-Cu-Ca alloys, temperature range and phase transitions during solidification.

Alloy composition (wt%)	Phase transformations during UST	Cooling rate (°C/s)	UST temperature range	UST time (min)	Ref.
Zn-0.5Al	L → η-Zn	0.5	436–415 °C	3.0	
Zn-1.0Al			433–410 °C		
Zn-0.5Ca-1.0Cu	L → $CaZn_{13}$	0.5	620–420 °C	7.0	
	L → $CaZn_{13}$	4.0	600–420 °C	4.0	
	L → $CaZn_{13}$	4.0	600–450 °C	2.0	[66]

smaller crucible (850–900 g). To avoid oxidation of Ca-containing alloys, Zn-Ca-Cu alloys were melted under a protective gas environment (1 % CO_2 + SF_6) at 720 °C. The ultrasonic system was made of a piezoelectric oscillator (Sonics Model No. VCX1500, 20 kHz and 1.5 kW), operated at 40 % of maximum power in most of the experiments using a Ti alloy sonotrode (20 mm diameter). The UST temperature range of application and time duration are listed in Table 1. A detailed schematic of the experimental setup for UST can be found in the references [43,54]. Other experimental papers that support similar or different mechanisms are discussed in individual sections. For pure metals and specific alloy systems discussed in this review, the details of master alloys used, UST and metallographic preparations can be found in specific references.

3. Grain refinement of Zn-based alloys: Role of solute

Zinc is predominantly utilized in galvanizing applications to protect structural steel components against corrosion [81,83]. Zn is also commonly used as an alloying element in light metals and Cu-based alloys [83]. Zn-based alloys are attractive for their lower processing temperature, fluidity, good surface finish and corrosion resistance [84–86]. Because of their hexagonal, densely packed crystal structure and the associated lack of desired mechanical properties, most Zn-based alloys are die-cast for small non-structural parts [87]. Foundry Zn alloys contain Al as the primary alloying element, with concentrations ranging from 4 wt% (hypo-eutectic alloys) to 27 wt% (hyper-eutectic alloys) [84].

Fig. 4 shows the cooling curves, macrostructures, and microstructure results of pure Zn in the as-solidified condition and after UST is applied at a range of temperatures specified in the respective cooling curves by start and end points [81]. Fig. 4(a_1-a_3) show the cooling curve and grain structure of high purity Zn without UST. In the as-solidified condition, grain growth starts from the mould wall regions (side and bottom walls) and extends to the centre of the casting with an average grain length of 8.8 ± 3.7 μm. In addition, a columnar grain zone was found in the top region of the casing where the melt is exposed to air (8.3 ± 1.9 mm); however, this zone occupies a relatively smaller area compared to the grain growth observed from the side walls of the mould [54]. Fig. 4(b_1-b_3) show the cooling curve during UST at the starting temperatures of 450 °C, applied for nearly 9 min during solidification. The macrostructure in Fig. 4(b_2) shows two distinct zones containing columnar and equiaxed grains. These columnar grains are aligned perpendicular to the mould wall with limited lateral growth and are finer than the columnar grains seen in Fig. 4(a_2). The microstructure observed from the equiaxed region is shown in Fig. 4(b_3). The grains are equiaxed yet display a dendritic growth with an average grain size of 422 μm. Interestingly, when the UST temperature is decreased to 440 °C (Fig. 4(c_1)), the columnar grains from the mould were eliminated, as shown in Fig. 4(c_2), and the microstructure shows finer non-dendritic grains.

The observations related to the fine columnar growth (Fig. 4(b_2)) were not observed in pure Mg for similar casting conditions [78]. The grains observed in pure Zn after UST at 440 °C are significantly finer than those in pure Mg and, clearly, this refinement in pure Zn is associated with UST applied at a lower temperature range. Fragmentation of dendrites from the columnar grains could explain the equiaxed zone observed in Fig. 4(b_2); however, the non-dendritic equiaxed grains without significant growth of columnar grains from the mould wall observed in Fig. 4(c_3) can only be explained by a nucleation mechanism.

Fig. 5(a and b) show the cooling curves of hypo-eutectic Zn-(0.5 and 1.0)Al alloy before and after UST. UST was applied at 20 °C above the liquidus temperature of the alloys and terminated after 3 min (indicated as start and end in Fig. 5(b)). The resulting macrostructures are shown in Fig. 5(c and d) for Zn-0.5Al alloy before and after UST, respectively. A comparison of Fig. 5(c) with the macrostructure of pure Zn (Fig. 4(a_2)) indicates that the addition of 0.5 wt% Al resulted in excellent grain refinement in the as-cast condition. The grain structure was uniform throughout the cross-section, with equiaxed grains having an average size of 313 ± 37 μm (Fig. 5(e)). Studies by Liu et al. have also noted a similar refinement tendency in the as-cast condition with the addition of Al, Cu, Mg [88] and Ag [89] to Zn, resulting in excellent grain refinement. Notably, this considerable grain size reduction (from over 1000 μm for the as-cast pure Zn to less than 200 μm) has occurred at lower addition levels of alloying elements, typically between 0.2 and 0.4 wt%

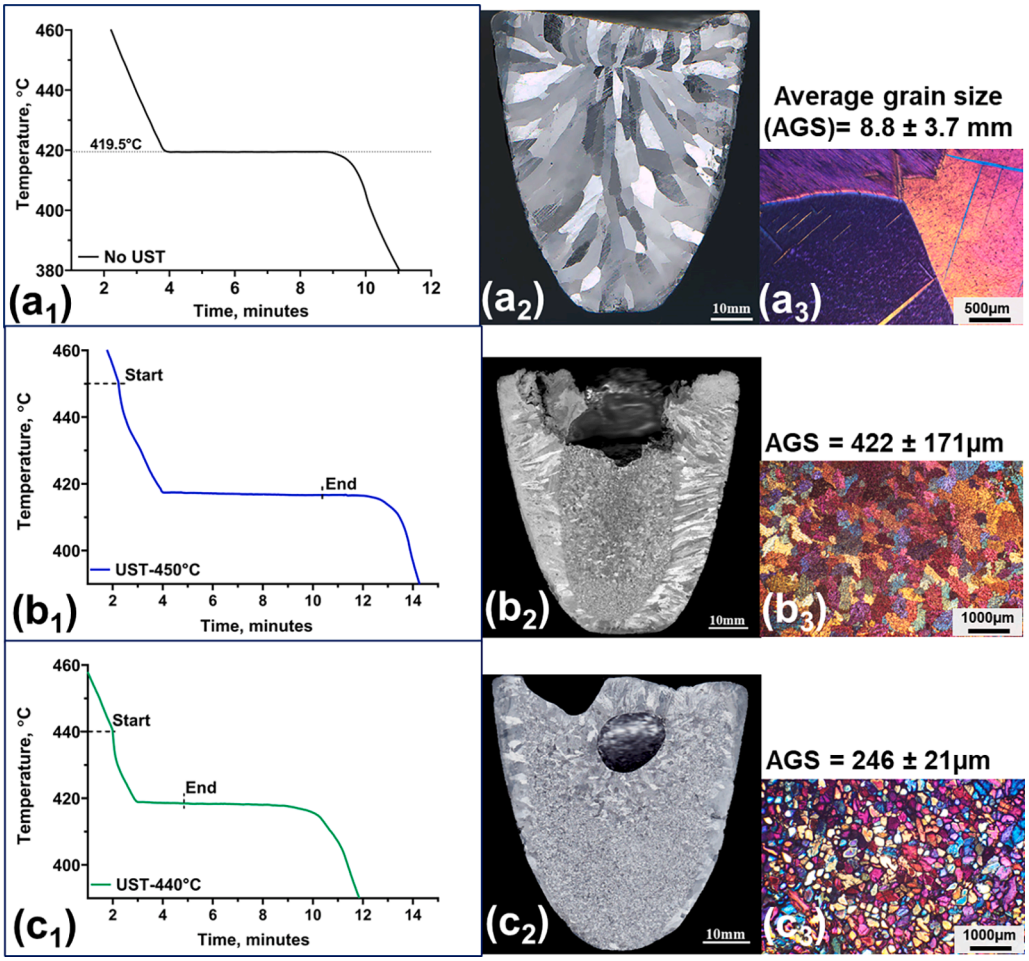

Fig. 4. Cooling curves (a_1, b_1, c_1), macrostructures (a_2, b_2, c_2) and microstructures (a_3, b_3, c_3) of high purity Zn without UST (a_1, a_2, a_3) and after UST applied from 450 °C (b_1, b_2, b_3) and 440 °C (c_1, c_2, c_3) respectively [54,81].

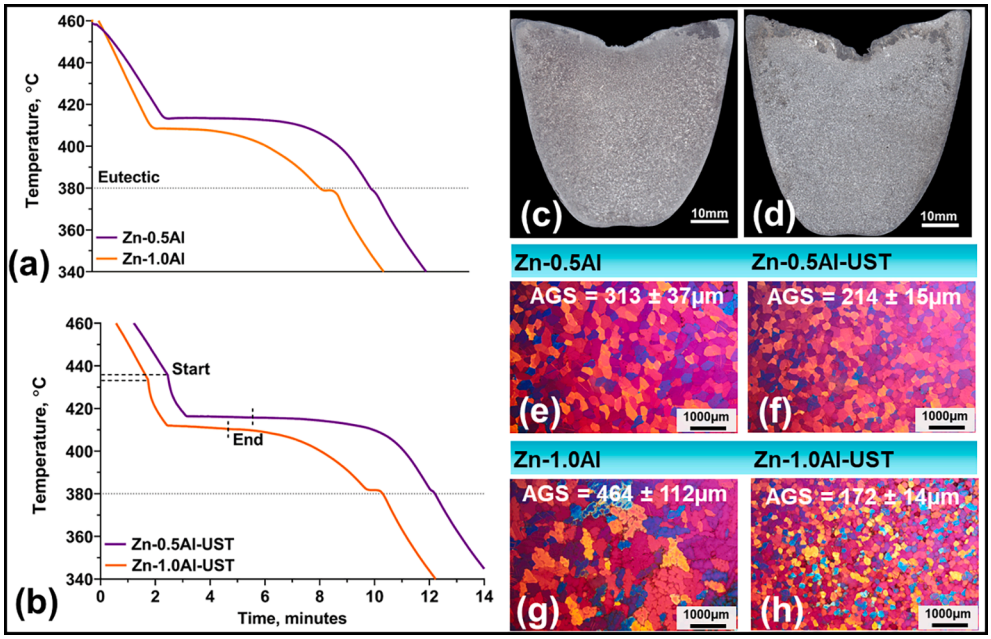

Fig. 5. Cooling curves of Zn-0.5Al and Zn-1.0Al alloy without UST (a) and after UST (b). Macrostructures of Zn-0.5Al alloy before (c) and after UST (d). Microstructures of Zn-0.5Al (e, f) and Zn-1.0Al (g, h) alloys without UST (e, g) and after UST (f, h).

[90,91]. UST during solidification improved the refinement further, as shown in the microstructure (Fig. 5(f)). However, the difference is barely noticeable from the macrostructure (Fig. 5(d)), and the improvement is marginal (214 ± 15 μm) when considering the refinement produced by the addition of Al alone. The grain size increased to 464 ± 112 μm and became dendritic when the Al concentration was increased to 1.0 wt% (Fig. 5(g)). The refinement produced by UST for Zn-1.0Al alloy for the same temperature range is finer and non-dendritic. An important and noteworthy observation is that when the casting conditions already promote fine and equiaxed grains, UST during solidification offers only a moderate improvement (Fig. 5(e and f)). Considering the grain refinement produced by the lone addition of Al in the as-cast condition, the refinement mechanism after UST could be related to nucleation enhancement.

Fig. 6 summarizes the important observation for UST grain refinement in pure metals and alloys containing solute and potent particles. When potent particles and solute with high GRF are present (Mg-1.0Zr alloy [43,53], Al alloys added with Al-Ti-B master alloy [22,23]), the grain refinement is significant (<100 μm) compared to the cases where low solute (Mg-3.0Zn [79], Al-2.0Cu alloys [77]) and impotent particles (Mg-1.0Zr-0.2Al-0.01Be [80], Al-Si-Ti alloys [29]) are present in the alloy. Alloys with higher solute contents that solidify dendritically in the as-cast condition results in better grain refinement after UST (Mg-6.0Zn [79] and Zn-1.0Al alloys). Further additions of solute or potent particles could reduce the grain size in these alloys. Therefore, when higher solute and potent particles are present, heterogeneous nucleation is enhanced by utilizing the physical effects of cavitation and streaming. However, when pure metals are subjected to UST, temperature-dependent grain refinement was noted (Fig. 4(c_3)). Clearly, a shift occurs from alloy chemistry-induced refinement to physical modes of refinement (separation mechanisms), where a low-temperature application of UST produces better refinement. This grain formation will be further explored in later sections.

4. Refinement of primary $CaZn_{13}$ intermetallic phases in Zn alloys: Effect of cooling rate

Recently, there has been a substantial increase in Zn alloy research due to their potential applications as degradable implant metal. In this application, Zn was combined with biocompatible alloying elements such as Ca, Cu and Fe, etc. These new alloys present additional challenges due to the formation of hard, brittle and coarse primary intermetallic phases in their as-cast structure [92–95]. Fig. 7 presents an example of a Zn-1.0Cu-0.5Ca alloy designed for biomedical application by the authors and describes the results of the application of UST to refine the primary $CaZn_{13}$ phase [66,82]. Without UST, the cooling curves in Fig. 7(a) indicate the precipitation of the peritectic $CaZn_{13}$ phase at 585–587 °C and the nucleation of η-Zn grains at 420 °C. A cooling rate of 0.5 °C/s was achieved by solidifying the alloy within the hot crucible in which the alloy was melted. A slightly higher cooling rate (4.0 °C/s) was promoted by transferring the alloy melt into another crucible preheated at 150 °C. UST-1 was applied from 620 °C and terminated before the onset of η-Zn without affecting the grains during solidification (at 420 °C). UST-2 and UST-3 were applied from ~ 600 °C due to the faster cooling rate and terminated at 420 °C and 450 °C, respectively. For UST-3, the alloy melt was immediately poured into a steel mould to arrest any further growth of the intermetallic phases and to compare the refinement produced by solidifying the alloy in the crucible (UST-2).

Fig. 7(b) shows that the primary dendrites of $CaZn_{13}$ phases without UST are long, measuring over 500 μm. Several remelted pieces are dispersed inside the matrix, each with a sharp interface that appears faceted, star-like, or petal-shaped. UST significantly refined the dendritic phases to become finer and polygonal phases without the dendritic structure in the microstructure, as shown in Fig. 7(c-e). Fig. 7(f) depicts the measurement of primary intermetallic phases before and after UST. The average size of primary intermetallic phases is decreased from greater than 100 μm to less than 20 μm, with reduced deviations noted for UST-2 and UST-3 due to faster cooling rates. SEM images in Fig. 7(g) show the representative image of the coarse dendritic structure of $CaZn_{13}$ phases in No UST-1 and after UST-3, for which the best refinement was noted.

The reduction in the size of primary intermetallic phases is attributed to the fragmentation effects of cavitation bubbles and fluid flow caused by acoustic streaming, along with the possibility of impurity (oxide) particles assisting nucleation [40,41]. Interestingly, the results in Fig. 7 showed that the finer structure after UST is associated with a higher cooling rate. The best refinement was noted for UST-2 (4 min at 4.0 °C/s) and UST-3 (2 min at 4.0 °C/s) compared to UST-1 (7 min at 0.5 °C/s) during solidification. It is reasonable to assume that a longer treatment time could enable more fragmentation of solid phases by cavitation events along with acoustic streaming. However, solidification conditions, such as the cooling rate, in this case, play a greater role in achieving the best refinement. The mechanisms for this refinement will be detailed in the later section.

5. Understanding the formation of non-dendritic/spherical grains

Considering Fig. 4(c_3) and Fig. 5(f, h), one of the main reasons to support the mechanism of nucleation during UST in pure metals and alloys is due to the formation of fine, non-dendritic/spherical grains, although in most cases, the nucleation particles are unknown/not characterized. This section will summarize the important efforts and

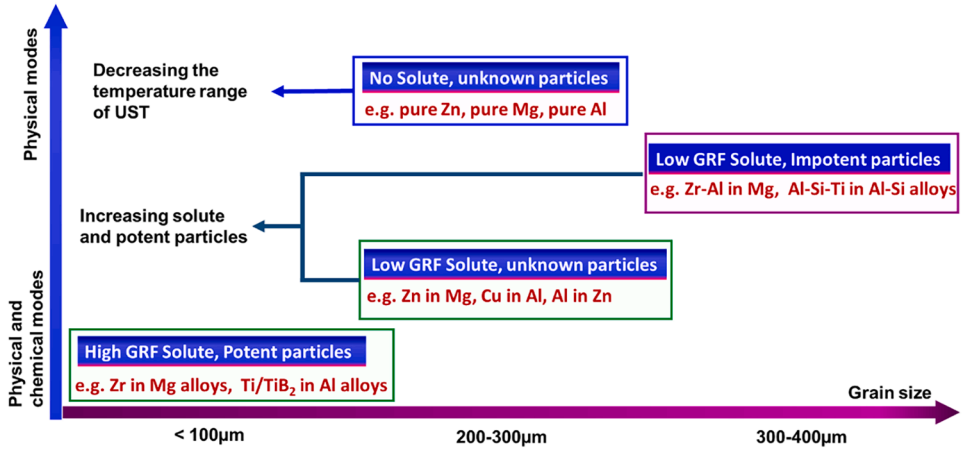

Fig. 6. Role of solute, potent, impotent (or unknown) particles and temperature range of UST influencing grain refinement in pure metals and alloys.

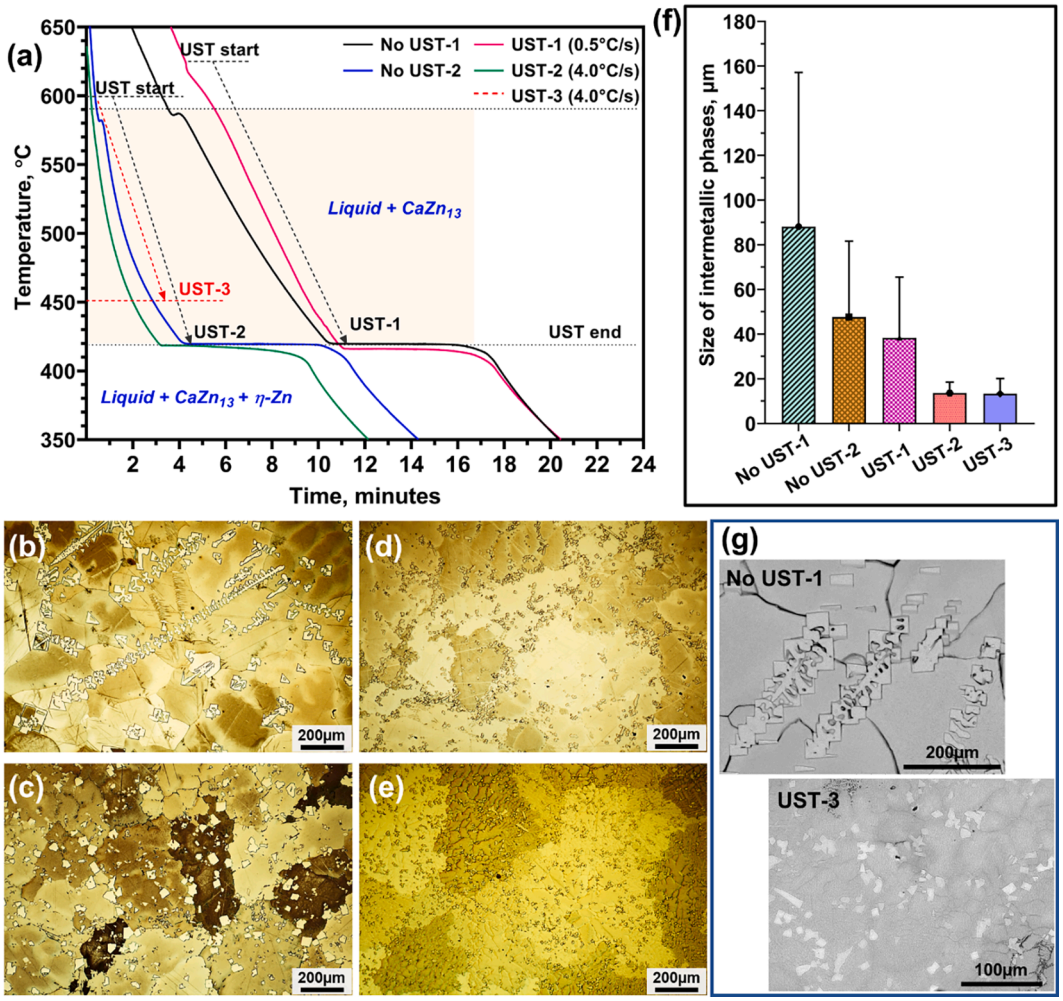

Fig. 7. (a) Cooling curves of Zn-1.0Cu-0.5Ca alloy in the as-cast condition and after UST at two different cooling rates (0.5, 4.0 °C/s) showing the temperature range of UST (UST-1 to UST-3). Microstructures images showing the $CaZn_{13}$ primary intermetallic phases (b) without UST, and after (c) UST-1, (d) UST-2 (e) UST-3 respectively. (f) The average size of $CaZn_{13}$ phases before and after UST at the specified temperature range. (g) SEM images show the coarse, dendritic morphology of $CaZn_{13}$ phases before UST (No UST-1) and the best refinement achieved after UST-3 with finely dispersed polygonal phases [66,82].

attempts made to capture and characterize the origin of the non-dendritic fine grains through dedicated experiments of UST applied during solidification.

5.1. Melt quenching experiments and castings with gauze barrier inserts

The schematic of the solidification arrangement in a clay-graphite crucible is shown in Fig. 8(a) and the corresponding cooling curve in Fig. 8(b) for the Al-2Cu alloy. The dashed lines represent the placement of stainless-steel gauze barriers inside the solidifying melt to capture and arrest the movement of grains. Three sets of experiments were conducted in this study. Firstly, the stainless-steel mesh was placed inside the molten alloy before UST, followed by the application of UST for nearly 4 min (from 40 °C above liquidus temperature) before the sonotrode was removed from the melt. Fig. 8(c) shows the macrostructure consists of fine grains within the enclosed mesh surrounding the sonotrode and these grains are fine and non-dendritic as demonstrated in the microstructure. The second set of experiments used a preheated silica tube (5.0 mm diameter) that was inserted into the melt beneath the sonotrode during UST at the specified times shown in Fig. 8(b) and then quenched immediately in cold water. The tube sampling points are marked as 1 to 4 in the cooling curve (Fig. 8(b)), corresponding to 0 s (at liquidus temperature), 20 s, 40 s, and 80 s (after reaching the liquidus temperature), respectively. In the third set of experiments, separate ingots were solidified at the same stopping points (points 1–4) to correlate and understand the formation of fine grains at various stages. Fig. 8(d) shows the macrostructure of the ingot samples and the microstructure of the quenched (tube) samples from points 1 to 4.

For the macrostructure refinement observed in Fig. 8(d) at point 1, UST was applied from 40 °C above the liquidus temperature and terminated at the liquidus temperature. The microstructure (tube sample) extracted from the top of the melt showed no equiaxed grains, with the dendritic structure prevalent in the quenched microstructure. This is because most of the fine grains during UST will be carried by acoustic streaming and settles to the bottom of the crucible forming an equiaxed zone after the vibration is stopped. This is observed in the macrostructure refinement in which a significant number density of equiaxed grains settles to create an equiaxed zone nearly occupying 50 % of the ingot's cross-section. After 20 s (at point 2), a few spherical grains start to appear in the microstructure sample, and the number density increases at 40 s (point 3). After 80 s (point 4), the microstructure consists of a maximum number of non-dendritic or spherical grains because more grains are being circulated at the top of the casting where the sample was taken. A clear distinction between equiaxed and coarse grains in the macrostructure is imperceptible after 20 s due to the formation of the mixed zone in the middle of the cross-section. However, after 40 s, the casting is almost filled with equiaxed grains. The spherical grains measured using the tube sample range from 70 to 100 µm, while the

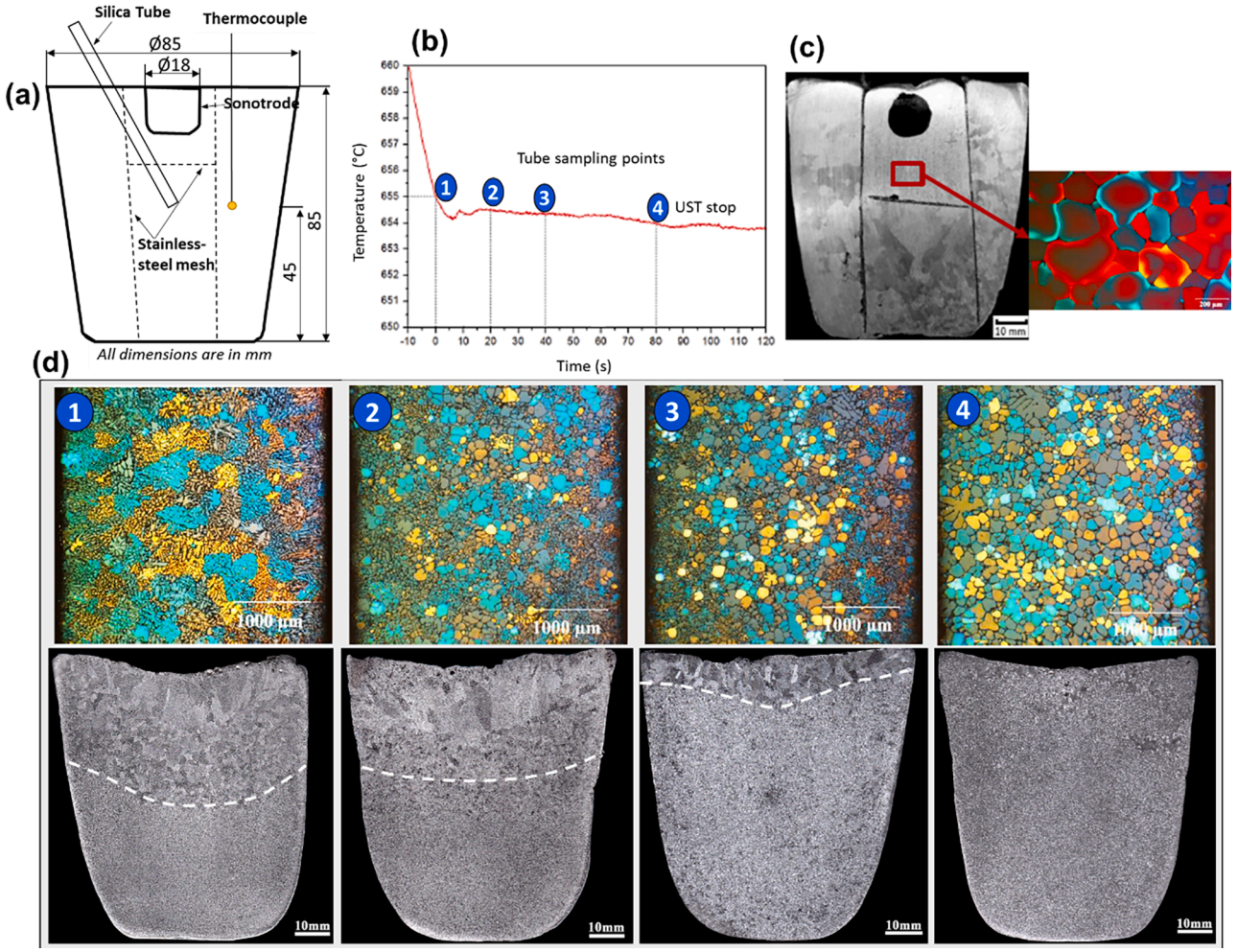

Fig. 8. (a) Schematic layout of the cross-section of the ingot indicating the locations of sonotrode, thermocouple, insertion depth of silica tube and stainless-steel mesh arrangement within the casting. (b) The cooling curve of Al-2.0Cu alloy shows the time at which the tube samples (points 1–4) were extracted during UST. (c) Macrostructure after UST with stainless-steel mesh trapping the fine grains within the mesh region. (d) Microstructure represents tube samples extracted at points 1 to 4 marked in (b) and separate solidification experiments conducted at these stopping points to observe the corresponding macrostructure refinement after UST [77].

equiaxed grains in the solidified ingot range from 150 to 200 µm. Thus, it can be understood that no significant growth happened between the quenched and solidified sample, and these findings reveal that the spherical and fine grains originate beneath or surrounding the sonotrode. Secondly, these grains do not appear to grow to a bigger size or become a dendrite grain; therefore, it is rational for the researchers to refer to this grain origin as nucleation instead of attributing such to the fragmentation mechanism [77].

5.2. *UST applied after the onset of solidification in pure Mg/Mg-6Zn alloy*

The results obtained from the methodologies adopted in Fig. 8 provided a better view of the formation of fine grains beneath the sonotrode and provided a basis for performing UST after the onset of nucleation during solidification, as shown in Figs. 9 and 10. UST was applied to pure Mg, Mg-6.0Zn alloy and pure Zn after the onset of the nucleation stage during solidification to capture the origin of fine grains at the sonotrode-melt interface. Fig. 9(a) shows the cooling curve of pure Mg. The UST duration (2 min) is highlighted at the end just before complete solidification. The sonotrode was vibrated in the air before inserting into the melt and this experiment has been repeated multiple times in pure metals (Mg [78], Al [55] and Zn [54]) to check the consistency and reproducibility of results. Fig. 9(b) shows the resulting macrostructure consisting of coarse columnar grains near the mould wall regions, because the onset of nucleation was undisturbed and the centre of the macrostructure was occupied by fine equiaxed grains (Fig. 9(c)). As observed in Fig. 8(c), the grains were produced beneath the sonotrode and then dispersed into the equilibrium melt creating a sharp columnar to equiaxed transition by impinging on the columnar grains (Fig. 9(d)).

Since the pure metal exhibits a large thermal arrest at a slow cooling rate, a significant amount of liquid melt still exists at equilibrium temperature and results in a refined structure (Fig. 9(b)). Therefore, a medium solute-containing Mg-6.0Zn alloy was subjected to UST after the onset of solidification. Due to the wider freezing range, UST was applied for 1 min after the onset of solidification and two thermocouples were used to measure the instantaneous melt temperature (TC_M) and temperature beneath the sonotrode (TC_S). The cooling curves of Mg-6.0Zn alloy during UST are shown in Fig. 9(e), with the insert images indicating the locations of thermocouples.

Placing the sonotrode just above the melt surface (~30–40 mm in height) warms the sonotrode tip to approximately 100–120 °C (TC_S). The thermocouple attached to the sonotrode revealed the increase in temperature when the sonotrode was immersed in the melt, and the temperature difference during UST was insignificant. The macrostructure in Fig. 9(f) shows that most of the cross-sectional area is occupied by coarse dendritic grains, except the region (marked by dashed lines) close

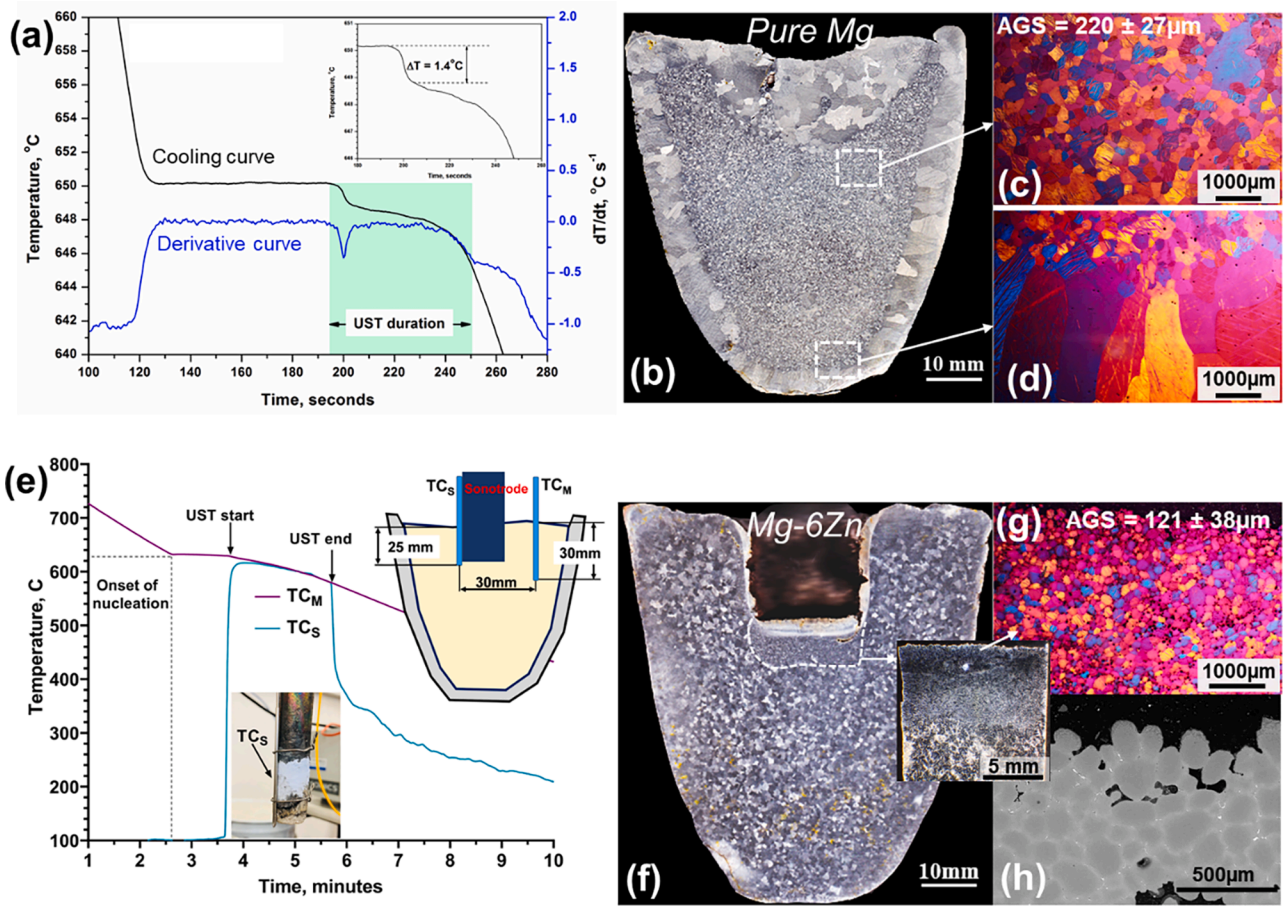

Fig. 9. Cooling curves (a, e), macrostructure (b, f) and microstructure refinement of (c, d) pure Mg and (g, h) Mg-6Zn alloy respectively when UST was applied after the onset of nucleation. Microstructures of pure Mg (c, d) and Mg-6Zn alloy (g, h) represents the fine grains observed within the equiaxed zone.

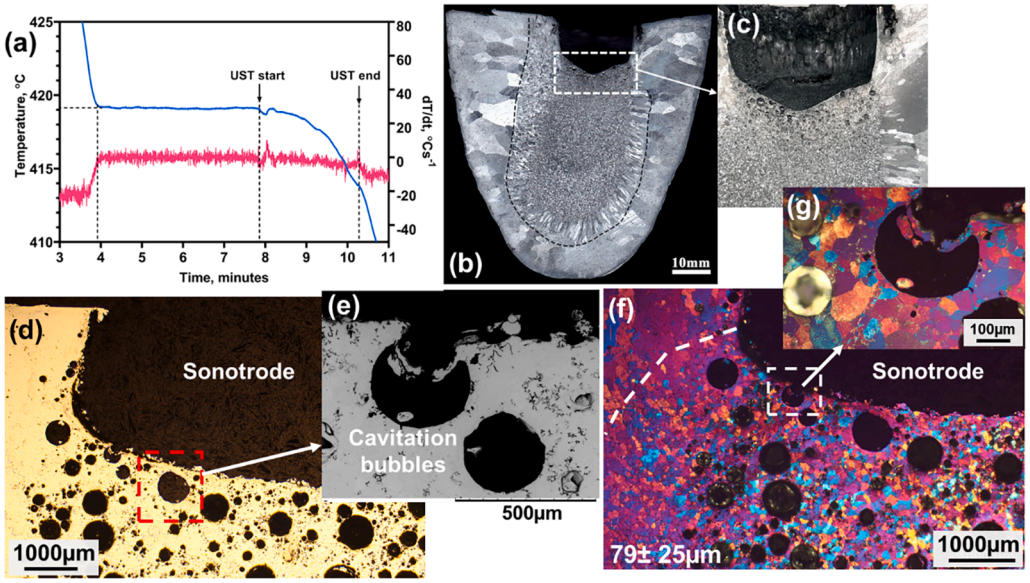

Fig. 10. UST applied to pure Zn after the onset of solidification: (a) cooling curve, (b, c) macrostructures, (d-g) shows the microstructures at the sonotrode-metal interface region for (d, e) cavitation bubbles and (f, g) grain refinement.

to where the sonotrode was immersed into the melt (~6 mm from the bottom surface of the sonotrode). The microstructure sample sectioned from the dashed region (inserted image in the macrostructure) shows much better insight into the origin of fine/spherical grains closer to the sonotrode. The average size of fine grains within the refined area is ~ 120 μm (Fig. 9(g)), and these grains originate mainly from the bottom surface of the sonotrode. The side surfaces of the sonotrode exposed to the melt can be disregarded as they show only coarse dendritic grains.

Fig. 9(h) shows the SEM image at the top region of the casting directly beneath the sonotrode consisting of several layers of fine grains with the solute layer in between the grains appearing as a bright network. The topmost layer in the SEM image shows numerous freely suspended grains, indicating that they might have separated due to vibration when the sonotrode was removed from the melt.

5.3. UST applied after the onset of solidification in pure Zn

Due to the limitations of the UST equipment in operating at high temperatures, the sonotrode could not be preheated to the melting/liquidus temperature of Al or Mg alloys. Thus, the occurrence of fine grains in Al and Mg alloys could be argued as a transient effect due to acoustic vibration using a low-temperature sonotrode (essentially a high-frequency vibrating rod). However, as demonstrated in Fig. 4(b_2) for pure Zn solidification, a mixed structure can be created at a slightly higher temperature range. Fig. 10 shows the results of solidification experiments conducted in pure Zn after the onset of solidification. Here, the sonotrode was preheated in a furnace at 600 °C for 2 hr, and UST was applied with 60 % power output just before complete solidification for 2 min (Fig. 10(a)). As shown in the macrostructure in Fig. 10 (b), the grains are still finer and equiaxed and occupy the centre of the castings' cross-section. Interestingly, in Fig. 10(c), the enlarged image of the macrostructure showed numerous porosities beneath the location where the sonotrode was placed in the melt. Bright-field optical image in Fig. 10(d) and SEM image in Fig. 10(e) show that these pores are spherical, and the size distribution (20–200 μm in diameter) corresponds well with the measured size of cavitation bubbles in Al-Cu alloy melt [38]. To the best of the authors' knowledge, capturing the cavitation bubbles in the solidified pure Zn ingot is unique compared to most of the UST solidification work reported previously other than the in-situ works. These cavitation bubbles are crowded near the sonotrode and are noticeable up to 25–30 mm from the bottom surface tip.

The grain structure observed at the sonotrode/melt interface is shown in Fig. 10(f and g). The average grain size observed in this region is much finer than pure Mg or Mg-6.0Zn alloy (Fig. 9). Fig. 10(f) shows a few large-sized bubbles along with several small ones surrounded by numerous fine grains. There is no significant difference in the size of fine grains, whether the grains are associated with large or small bubbles or in the regions where no bubbles are noted. Besides, the presence of fine grains above and below the bubbles (towards the sonotrode direction) indicates that these bubbles do not influence grain formation. Fig. 10(g) shows a high magnification image of a single bubble along with a solidified layer that was also separated from the sonotrode. It should be noted that cavitation can only occur if a considerable volume of liquid melt is present in the cavitation zone. Thus, the sonotrode can be assumed as hotter compared to Fig. 9, though the sonotrode can still act as a heat sink. From Fig. 10(g), it can be inferred that solidification or solid formation occurs locally surrounding/beneath the sonotrode, in which either vibration alone or together with cavitation can separate these solid layers as fine grains.

6. Grain refinement mechanisms: Origin of fine grains from the sonotrode / solidifying metal interface and the role of cavitation

Ultrasound-induced crystallisation (also called sonocrystallisation) has been studied in a wide range of organic liquids, including metallic melts, for grain refinement [96]. The earlier reports on the crystallisation phenomenon for grain refinement are largely studied in organic liquids [97,98]. During ultrasonic irradiation, bubbles are created from the impurities present within the melt, and after reaching a critical resonant size, these bubbles implode (collapse) causing both chemical and physical effects inducing crystallisation [96,98]. The chemical effects include a significant change in local temperature, pressure and cooling cycles in the vicinity of bubble collapse [99]. Generation of high-speed micro-jets with very high velocity, shock waves after collapse near a solid substrate and inter-particle collisions are responsible for inducing physical effects and fragmentation (also known as sonofragmentation) [96–98]. The aim of this review is not to present the ideas or discuss the mechanisms reported for ultrasonic crystallisation in organic liquids, as there is still considerable debate about the chemical and physical effects of UST [96,98,99]. We will only attempt to examine the possibilities of the theories and concepts extended to metallic melt for grain refinement behaviour.

The formation and collapse of bubbles were expected to increase the local temperature and pressure estimated using the Clausius-Clapeyron equation, substantially increasing the nucleation density [47]. For a cavitation pressure of 200–1000 atm, the temperature change or undercooling in pure Al melt has been estimated to vary from 1.5 to 7.4 °C [100]. Although in-situ studies during alloy solidification do not reveal such a nucleation phenomenon [34,35,39], the formation of fine grains observed in Fig. 9 and Fig. 10 could not be explained using fragmentation theories. The next possible argument for supporting nucleation on impurity or oxide substrates arises from the fact that intense convection generated by acoustic streaming can promote a nearly flat temperature gradient during solidification [28]. This mechanism was adopted from melt processing techniques that use mechanical stirring or intensive shear mixing [50,101] solidification, where the resultant microstructure shows non-dendritic or spherical grains at high-stirring speeds (due to turbulent flow) [48,49]. In both these nucleation mechanisms, undercooling generated by pressure pulses or by intense convection plays a major role in nucleation. One of the underexplored mechanisms for UST is the high-frequency vibrations responsible for continuously producing grains from cold surfaces (vibrating sonotrode) due to a larger thermal undercooling [12]. During UST, the sonotrode placed over the melt surface can deliver significant thermal undercooling and is capable of generating fine grains continuously from the surface of the vibrating rod [54,56]. Ohno [69,70] coined this type of grain formation as a separation mechanism, in which fine grains are continuously produced from the cold surfaces (stirring rod, mould wall, vibrating rods) during agitation. It should be noted that several pieces of crucial information behind the grain origin through the separation mechanism are still elusive. Some of these include (i) the thickness of the solidified phase initially formed on the mould wall or vibrating rod, (ii) how the vibration splits the solid layers (either in one or as multiple solid phases), (iii) their original size at the onset of solidification, (iv) rate of production or separation and (v) survivability or growth for a given alloy composition. Although several questions need in-depth investigations, the following sections are presented to propose a possible mechanism for creating spherical grains during UST.

Fig. 11 aims to provide a simplified insight into the formation of fine grains, explaining the role of ultrasonic vibration and cavitation bubbles. Fig. 11(a) shows a mesh-like regular structure of capillary waves of liquid layer for a 20 kHz device operated at 1 W (low) power to capture the wave patterns [61]. The distance between immediate crests was 155 μm, and the droplet size produced was approximately half of the capillary wavelength. Fig. 11(b and c) shows that the regular wave pattern at a critical flow rate changes to irregular shapes (triangular or pentagon shapes) with an increase in flow rate and after the occurrence of cavitation (Fig. 11(c)). Fig. 11(d) shows the erosion pattern of the Ti sonotrode (20 mm diameter) after UST in Al alloy, exhibiting irregular patterns resembling Fig. 11(c). Though it is an oversimplification to extend the principles of atomisation or droplet formation effect to grain refinement during solidification, Fig. 11(e) shows the correlation of droplet size with the grain size observed for various alloys from the present work and reported elsewhere for Al, Mg and Zn-based alloys [56]. The average grain size was found to lie within the droplet size range of liquids reported for a 20 kHz device. The main difference is that the liquid droplets ejected from the sonotrode are replaced with solid layers (~70–100 μm thickness) that are separated by capillary excitation. Assuming a layer of solidification occurs beneath the sonotrode, the concept of capillary excitation was responsible for the separation of

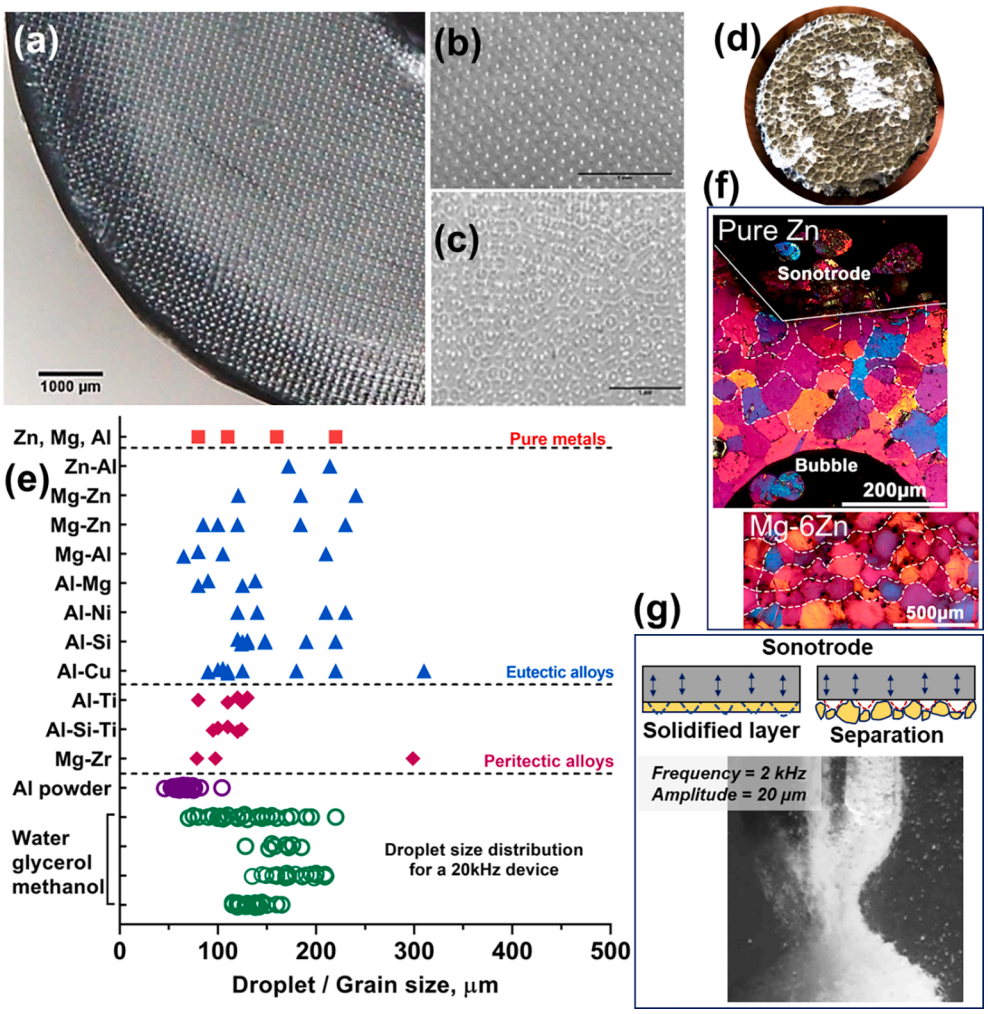

Fig. 11. Standing capillary waves showing (a) regular pattern on the surface of the atomiser and the change in patterns observed at (b) critical flow rate and (b) after cavitation and ejection of droplets [61]. (d) The erosion pattern obtained for Ti sonotrode (20 mm diameter) after UST in Al melt resembles the pattern shown in (c). Comparison of grain size reported for several Al, Mg and Zn-based alloys under similar casting conditions to the droplet sizes reported for a 20 kHz device [56]. (f) Microstructures of pure Zn and Mg-6.0Zn alloy just beneath the sonotrode showing the grain structure. Dashed lines represent the separation of grains in horizontal and vertical directions due to vibration. (g) A simplified schematic of the solidification layer beneath the sonotrode and its separation during UST. The insert image from a real-time study shows the chill crystals of NH_4Cl–70 wt-%H_2O alloys surrounding the vibrating rod as an example for the visualisation of the separation mechanism [102].

grains at a characteristic distance along the horizontal direction (crest-to-crest distance of 155 µm without cavitation [61]). The vibration along the principal direction (amplitude of vibration) is responsible for the separation along the principal direction of propagation. For example, Fig. 11(f) shows the microstructure of pure Zn and Mg-6.0Zn alloy observed at the sonotrode/metal interface. The dashed lines are actually grain boundaries indicating that these grains are separated along the horizontal and vertical directions. The grains observed in Mg-6.0Zn alloy without any cavitation bubbles show a certain degree of continuity along the horizontal direction. This pattern is difficult to observe in pure Zn (Fig. 11(f)) because of the formation of cavitation bubbles and the implosion events occurring in the cavitation zone. Thus, the grain size typically ranging from 80 to 150 µm in most of the solidification experiments is produced by the excitation of vibrations (capillary excitation) at a characteristic distance, causing periodic solidification and ejection of grains. It should be noted that this mechanism of fine grain formation requires the formation of a solid layer (due to the thermal undercooling) beneath the sonotrode. The importance of thermal undercooling and cold zones in a casting condition is detailed in a later section.

A simplified schematic is provided in Fig. 11(g) for the capillary excitation. Either a regular (Fig. 11(a, b)) or irregular vibration with cavitation (Fig. 11(c)) can break the solid layer into finer grains. Once the solidified layer is removed, this is transported by acoustic streaming into the melt, exposing the sonotrode with a fresh layer of liquid (equilibrium) melt and causing the second cycle to occur. In addition, acoustic streaming generates a low temperature gradient throughout the melt where the liquid is undercooled so that the new grains do not remelt or grow into a dendrite. This mechanism is indeed hard to visualize for vibrations occurring at 20 kHz frequency. The insert image in Fig. 11(g) is an example of visualising the crystal formation surrounding the vibrating rod (2 kHz frequency) in a transparent analogue [102]. Note that several aspects such as liquid layer wetting the sonotrode, solid formation, effect of viscosity or any other factors needs a much more detailed study to understand this UST grain refinement process. The formation of cavitation bubbles with or without implosion can assist the refinement further by accelerating the separation of the solid layer into multiple grains or to smaller sizes, however, it may also interfere with solid formation.

Finally, the aim of Fig. 11 is to explain why spherical, non-dendritic grains are observed for pure and eutectic alloys and how they formed during UST. These grains cannot be attributed to enhanced nucleation on suspended impurity particles after an implosion event creating a change in pressure or low-temperature gradients [44–46,75,103].

7. Refinement of primary intermetallic phases

The onset of crystallization of primary intermetallic phases occurs at a relatively higher temperature (above the onset temperature of grains solidification) and depends on the alloy composition. Due to a relatively larger liquid fraction, cavitation and acoustic streaming-induced fragmentation mechanisms are expected to dominate the refinement of the primary intermetallic phases during UST [43,73]. There are few prominent alloy systems in Al and Mg alloys that solidify with primary

crystalline or intermetallic phases, including primary Si [103,104], Al_3Zr [105], Al_3Ti [106], Al-Zr-Ti [107], Al_3Fe [73], Al_3Ni [73], α/β- Fe intermetallics [108] and those with grain refiner particles such as TiB_2 in Al alloys and Zr particles in Mg alloys [43]. In addition to the fragmentation effects, activation of oxide particles has also been considered as one of the possible mechanisms [43,106]. Water model experiments with suspended particles are used to understand the modes of fragmentation caused by cavitation bubbles, shock waves due to the cavitation cloud beneath the sonotrode and acoustic streaming [37]. For a given volume, it has been verified with water models and simulations that fluid flow and recirculation flow caused by acoustic streaming continuously expose the particles to the cavitation zone to produce more fragments [36,37]. Fig. 12(a) shows the best refinement conditions reported for the primary intermetallic phases after UST. The extent of refinement from a 'no UST' condition to after UST is dependent on the temperature range of application, alloy composition, impurities and UST time. Thus, making comparisons of the extent of refinement between alloy systems is challenging.

Since the physical effects of UST dominate intermetallic refinement, it is expected that a longer treatment time during solidification could facilitate finer fragments or better refinement. However, in Fig. 7, UST applied at a faster cooling rate of 4.0 °C/s for 2 min yields the finest average size of 13 μm for $CaZn_{13}$ phases compared to a slower cooling rate (0.5 °C/s) UST for 7 min (average size of 38 μm). This further reveals the importance of solidification conditions and understanding the precipitation of intermetallic phases when external fields are applied.

Fig. 12(b) shows the schematic of two cooling conditions at the onset of nucleation of primary $CaZn_{13}$ phases (~585 °C). Unlike in Fig. 11 where the sonotrode acts as a heat sink, the cold zones in Fig. 12 (b) are located predominantly at the locations closer to the mould walls on the side and at the bottom of the crucible. Fine columnar grains observed at the mould wall in Fig. 4(b_2) exemplify the high-temperature UST triggering nucleation along the mould wall regions at the onset temperature. Thus, after acoustic streaming establishes a uniform flow inside the melt, the temperature gradient from the mould wall to the centre of the solidifying melt is relatively flat for the slow cooling condition compared to the fast-cooling state. Due to a flat temperature gradient, slow cooling conditions start to nucleate a low number density of primary phases with a noticeable growth in lateral directions (inferred from their larger average size). Finer and a larger number density of precipitates are expected to form in fast cooling conditions with reduced lateral growth, as shown in the schematic (Fig. 12(b)). At slow cooling conditions, acoustic streaming can separate these phases from the wall only after significant growth is attained in principal and lateral growth directions resulting in the overall increase in the average size of phases. After separation from the mould wall, and if cavitation is powerful enough to induce further fragmentation, one can expect an equivalent or nearly finer size for UST-1 similar to UST-2/UST-3. Although it is indisputable that cavitation could produce fragmentation of the primary phases, casting conditions such as cooling rate still promoted the finest refinement. It is worth noting that reducing UST time from UST-2 (4 min) to UST-3 (2 min) for a constant cooling rate (4.0 °C/s) also produces similar refinement, indicating that finer phases are associated with faster precipitation at the onset of solidification and separation by acoustic streaming. Since the activity of cavitation events is found to decrease exponentially with respect to the distance from the sonotrode [105,109], intermetallic refinement is controlled by cooling rate and acoustic streaming-induced fluid flow.

8. Relevance of mechanism understanding to commercial processes (DC casting process) and the role of cold zones in a casting condition

Figs. 4 and 5 demonstrate the grain refinement of UST as a function of alloy composition, while Figs. 8-10 describe the origin of fine grains beneath the sonotrode. In all these lab-scale experiments, the sonotrode was inserted through the top surface of the melt, where a significant heat extraction occurs from the top surface of the melt. Fig. 13(a) schematically shows the cold zones (shaded regions) along the mould wall, melt surface and beneath the sonotrode. Even though preheating is applied to the sonotrode in some experiments, heat extraction through the sonotrode is inevitable, and the sonotrode induces a significant thermal undercooling in the melt. For instance, the sonotrode was not preheated in Fig. 9(e), and the temperature of the sonotrode just before inserting it into the liquid metal (at 620 °C) was approximately measured as ~ 100–120 °C. Preheating of the sonotrode reduces the extent of this thermal undercooling, however, this undercooling is much more significant than the undercooling stated for pressure pulse theories or intense convection generated by stirring techniques. As shown in Fig. 11, high-frequency vibrations can produce a greater number density of fine grains and fill the entire volume of small-scale castings within 2 min of UST (cooled at 1.0 °C/s). This also applies to Zn-based alloys. However, the macrostructure in Fig. 4(b_2) is an interesting case where UST applied from 450 °C generates fine columnar grains from the mould wall, indicating that the sonotrode region is hotter than the mould wall. Also, it was found that in pure Zn solidification, the grain formation explained using Fig. 11ceases after 4 min (at 440 °C) because the sonotrode becomes hotter [81].

For commercial processes such as the DC casting process, it is not possible to maintain the sonotrode at a lower temperature because the hot melt will be continuously fed over the top of the casting. The solidification happens along the water-cooled mould placed on the sides of

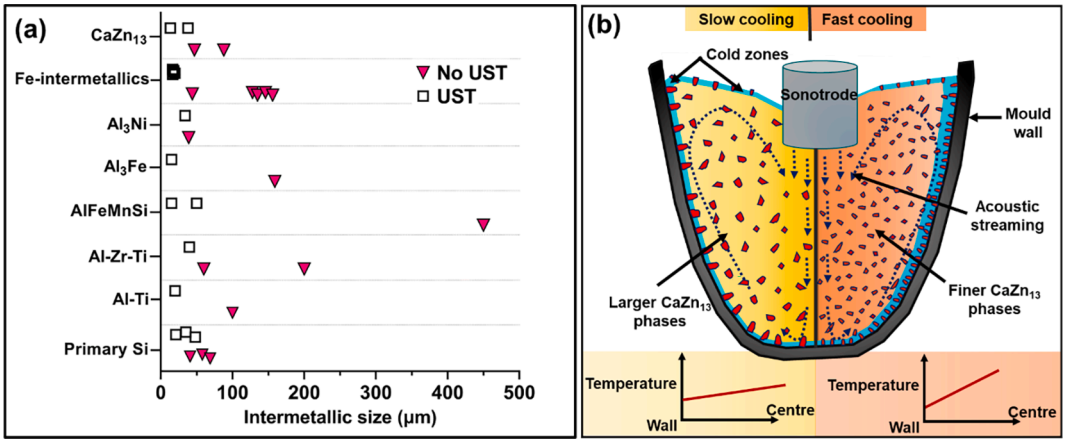

Fig. 12. (a) Refinement of a few common primary intermetallic phases reported in Al and Zn-Ca-Cu alloys after UST [73,103,104,106–108]. (b) Schematic of the mechanism of refinement for primary intermetallic phases at different cooling rates during UST [66].

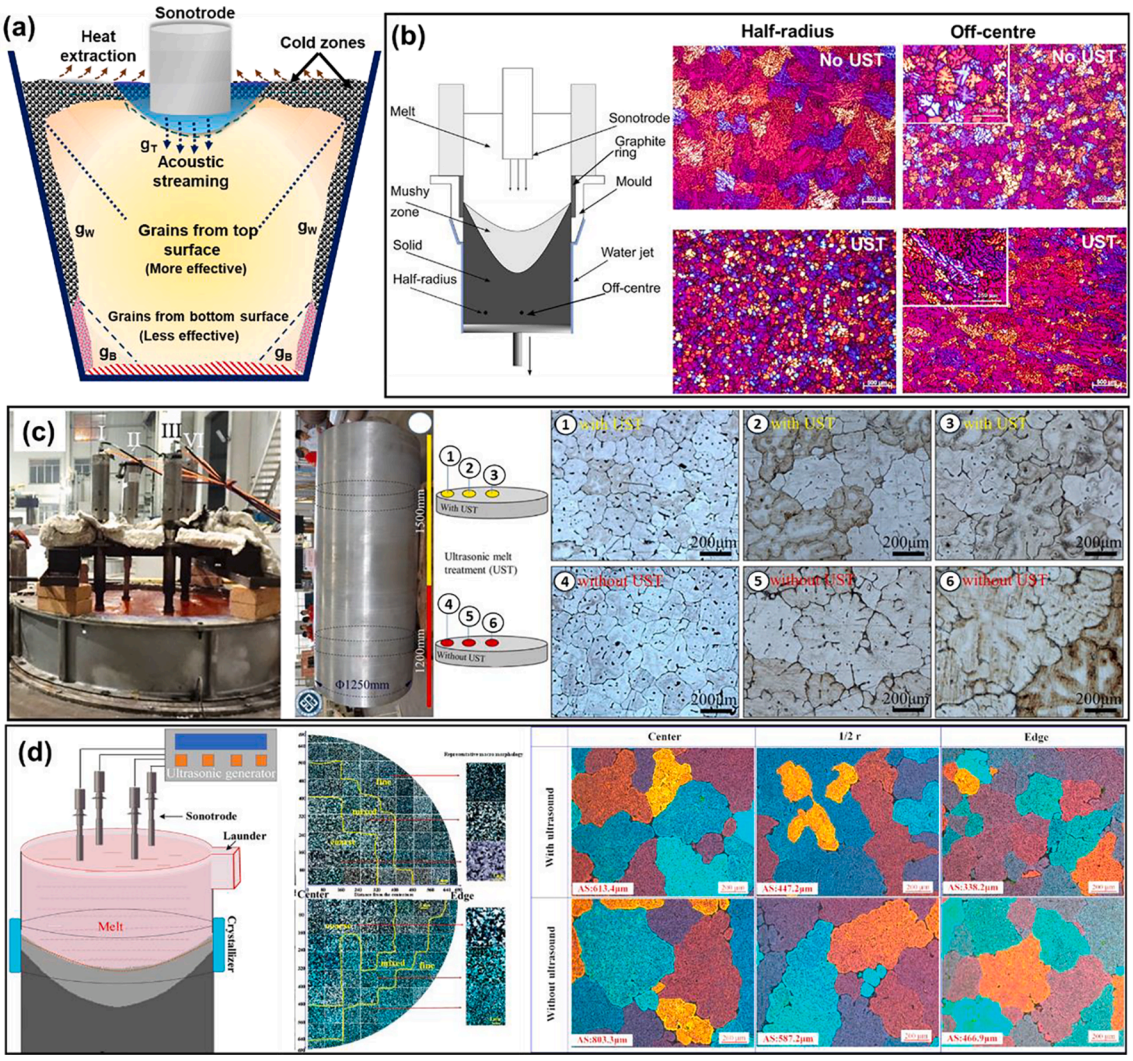

Fig. 13. (a) Cold zones at the onset of UST solidification in lab-scale experiments. (b, c, d) UST is used in the commercial direct chill casting process with one or multiple sonotrode and the corresponding microstructures showing the refinement before and after UST [30,67,110].

the casting and continuously pulled in the centre at a specific casting speed [30]. Several studies investigated the application of UST to the DC casting process to predict and improve the flow conditions, temperature gradients and microstructure refinement [30,31,67,110]. Fig. 13(b-d) shows some examples in the DC casting of Al alloys, and this discussion is focused only on the formation of fine grains. Fig. 13(b) shows the application of UST to DC casting (155 mm diameter) of Al6061 Al alloy [110]. It is interesting to note that when the sonotrode was submerged to the level of the graphite ring, finer grains are observed at the half-radius position after UST and the middle region shows elongated grains as shown in the microstructure. The refinement observed at the half-radius position faded when the sonotrode was further moved upwards (100 mm above the graphite ring). Fig. 13(c and d) show the application of UST to ultra-large ingots (1250 mm diameter, 2700 mm in length [67] and 1380 mm diameter, 4600 mm in length [30]). Due to the large diameter of the ingots, 4 sonotrodes were used to treat the melt, as shown in Fig. 13(c and d). The microstructure refinement reported in these studies (Fig. 13(c and d)) before and after UST was insignificant compared to the grain size refinement achieved with the small-scale experiments.

One of the key issues here is the mechanistic understanding of the origin of fine grains. Typically, most in-situ solidification studies state that fine grains are produced by fragmentation/remelting of dendrite due to fluid flow or cavitation, subsequently generating grains from the mushy zone, which is expected to produce a significant refinement in DC casting conditions. Although fragmentation creating dendrites from the mushy zone cannot be ignored entirely, this is insufficient to generate significant refinement. In the DC casting conditions, finer grains can be generated when the sonotrode is placed near the mould wall where the onset of solidification occurs (Fig. 13(b)) than placing several sonotrodes in the centre of the melt (Fig. 13(c and d)). Thus, as marked in Fig. 13(a), for small-scale castings, the most effective positioning for producing fine grains is the top surface of the melt, while for DC castings, this is close to the mould wall locations. Relying on acoustic streaming or cavitation to produce dendritic fragments (from the mushy zone) was considered the least effective method to produce a higher number density of fine grains, which is evident in the DC casting grain refinement.

In summary, agitation in the form of cavitation, vibration or fluid flow can produce fine grains only if the external fields are positioned close to cold zones in the casting condition where the onset of solidification occurs. In lab-scale conditions, the sonotrode itself acts as a heat sink forming a cold zone surrounding the sonotrode, whereas, in DC casting, the cold zone is shifted to the regions close to the mould wall. A low-frequency magnetic field applied through the mould wall producing excellent refinement from the edge to the centre of the ingot is the best example to understand the effect of the mould wall-induced fine grains in the DC casting condition (200 mm diameter) [111].

9. Summary and outlook

Ultrasonic processing of metallic melts during solidification has been critically reviewed for the mechanisms (nucleation and fragmentation of solid phases) and the casting conditions (cooling rate, cold zones in the casting, alloy composition) promoting refinement of primary intermetallic phases and grain structure. For any given temperature range of UST application, the presence of potent inoculant particles offered the best refinement mainly by increasing the number density of active nucleating substrates. UST solidification in pure metals and other (eutectic) alloy systems with dilute or higher solute contents exhibit a non-dendritic, spherical grain structure, which was often attributed to the enhancement of nucleation on oxide or impurity particles due to cavitation induced undercooling. A series of experiments were designed to find the origin of these fine grains using gauze barriers, melt quenching and applying UST after the onset of nucleation in eutectic alloys and pure metals. These experiments revealed that the non-dendritic, fine grains (size ranging from 80 to 150 μm for most alloys) are generated from the bottom of the vibrating sonotrode. Significant thermal undercooling induced by the cooling at the melt surface and regions closer to or beneath the sonotrode promote a local solidification. Cavitation or vibration could separate these grains from the sonotrode surface, while acoustic streaming disperses these grains throughout the remaining melt volume. The mechanism of grain separation from the sonotrode was explained using capillary excitation at the bottom surface of the sonotrode. Further exploration is needed to understand this grain formation mechanism because this effect generates excellent refinement in most alloys.

In contrast to the grain formation mechanism, finer primary intermetallic phases are greatly influenced by the cooling rate of solidification as nucleation is expected to occur along the mould walls. Acoustic streaming (fluid flow) plays a major role in causing their separation/remelting at the onset of nucleation. Because a higher number density of precipitation at faster cooling rates (4.0 °C/s) results in the finest average size of $CaZn_{13}$ phases for 2 min UST compared to a 7 min UST at a slower cooling rate (0.5 °C/s).

In lab-scale solidification conditions, cold zones are located at the top of the melt surface where the vibrating sonotrode can effectively produce finer grains. This cold zone is shifted to the locations close to the mould wall regions in the DC casting process. One or multiple sonotrodes, when placed in the centre of the melt, yield an insignificant refinement in the DC casting when compared to the refinement achieved by placing the sonotrode at the half-radius position. Therefore, in cases where the vibrating sonotrode could not act as a cold source, a relatively better refinement could be promoted by locating the vibrations or agitations closer to the cold zones where the onset of solidification occurs. The extent of refinement will be much better if the solidification occurs on the vibrating surface (with or without cavitation) than on the other surfaces elsewhere in the casting (e.g. mould wall in DC casting).

CRediT authorship contribution statement

Nagasivamuni Balasubramani: Conceptualization, Data curation, Investigation, Methodology, Visualization, Writing – original draft, Writing – review & editing. **Jeffrey Venezuela:** Formal analysis, Writing – review & editing. **Nan Yang:** Writing – review & editing. **Gui Wang:** Writing – review & editing. **David StJohn:** Validation, Writing – review & editing. **Matthew Dargusch:** Funding acquisition, Project administration, Resources, Supervision, Writing – review & editing.

Declaration of Competing Interest

The authors declare that they have no known competing financial interests or personal relationships that could have appeared to influence the work reported in this paper.

Data availability

No data was used for the research described in the article.

Acknowledgements

The authors acknowledge the funding support provided by the Australian Research Council Research Hub for Advanced Manufacturing of Medical Devices IH150100024, the ARC Discovery grant DP140100702 and the ARC linkage project LP150100950.

References

[1] Y. Li, H. Li, L. Katgerman, Q. Du, J. Zhang, L. Zhuang, Recent advances in hot tearing during casting of aluminium alloys, Prog. Mater. Sci. 117 (2021), 100741.
[2] M.A. Easton, M. Qian, A. Prasad, D.H. StJohn, Recent advances in grain refinement of light metals and alloys, Curr. Opin. Solid St M 20 (1) (2016) 13–24.
[3] E. Karakulak, A review: past, present and future of grain refining of magnesium castings, J. Magnesium Alloys 7 (3) (2019) 355–369.
[4] H. Shang, Z.L. Ma, S.A. Belyakov, C.M. Gourlay, Grain refinement of electronic solders: the potential of combining solute with nucleant particles, J. Alloy. Compd. 715 (2017) 471–485.
[5] Y.H. Cho, H.C. Lee, K.H. Oh, A.K. Dahle, Effect of strontium and phosphorus on eutectic Al-Si nucleation and formation of β-Al5FeSi in hypoeutectic Al-Si foundry alloys, Metall. Mater. Trans. A 39 (10) (2008) 2435–2448.
[6] D.G. McCartney, Grain refining of aluminium and its alloys using inoculants, Int. Mater. Rev. 34 (1) (1989) 247–260.
[7] D.H. StJohn, M.A. Easton, M. Qian, J.A. Taylor, Grain refinement of magnesium alloys: a review of recent research, theoretical developments, and their application, Metall. Mater. Trans. A 44a(7) (2013) 2935-2949.
[8] Y.H. Ali, D. Qiu, B. Jiang, F.S. Pan, M.X. Zhang, Current research progress in grain refinement of cast magnesium alloys: a review article, J. Alloy. Compd. 619 (2015) 639–651.
[9] D.G. Eskin, I. Tzanakis, F. Wang, G.S.B. Lebon, T. Subroto, K. Pericleous, J. Mi, Fundamental studies of ultrasonic melt processing, Ultrason. Sonochem. 52 (2019) 455–467.
[10] G.I. Eskin, Broad prospects for commercial application of the ultrasonic (cavitation) melt treatment of light alloys, Ultrason. Sonochem. 8 (3) (2001) 319–325.
[11] M.C. Flemings, Solidification processing, Metall. Trans. 5 (10) (1974) 2121–2134.
[12] J. Campbell, Effects of vibration during solidification, Int. Met. Rev. 26 (1) (1981) 71–108.
[13] C.J. Todaro, M.A. Easton, D. Qiu, D. Zhang, M.J. Bermingham, E.W. Lui, M. Brandt, D.H. StJohn, M. Qian, Grain structure control during metal 3D printing by high-intensity ultrasound, Nat. Commun. 11 (1) (2020) 142.
[14] D. Zhang, A. Prasad, M.J. Bermingham, C.J. Todaro, M.J. Benoit, M.N. Patel, D. Qiu, D.H. StJohn, M. Qian, M.A. Easton, Grain refinement of alloys in fusion-based additive manufacturing processes, Metall. Mater. Trans. A 51 (9) (2020) 4341–4359.
[15] D. Yuan, S. Shao, C. Guo, F. Jiang, J. Wang, Grain refining of Ti-6Al-4V alloy fabricated by laser and wire additive manufacturing assisted with ultrasonic vibration, Ultrason. Sonochem. 73 (2021), 105472.
[16] O.V. Abramov, Action of high-intensity ultrasound on solidifying metal, Ultrasonics 25 (2) (1987) 73–82.
[17] V. Abramov, O. Abramov, V. Bulgakov, F. Sommer, Solidification of aluminium alloys under ultrasonic irradiation using water-cooled resonator, Mater. Lett. 37 (1–2) (1998) 27–34.
[18] G.I. Eskin, Cavitation mechanism of ultrasonic melt degassing, Ultrason. Sonochem. 2 (2) (1995) S137–S141.
[19] X. Jian, H. Xu, T.T. Meek, Q. Han, Effect of power ultrasound on solidification of aluminum A356 alloy, Mater. Lett. 59 (2–3) (2005) 190–193.
[20] T.V. Atamanenko, D.G. Eskin, L. Zhang, L. Katgerman, Criteria of grain refinement induced by ultrasonic melt treatment of aluminum alloys containing Zr and Ti, Metall. Mater. Trans. A 41a (8) (2010) 2056–2066.
[21] T.V. Atamanenko, D.G. Eskin, M. Sluiter, L. Katgerman, On the mechanism of grain refinement in Al-Zr-Ti alloys, J. Alloy. Compd. 509 (1) (2011) 57–60.
[22] Y.F. Han, K. Li, J. Wang, D. Shu, B.D. Sun, Influence of high-intensity ultrasound on grain refining performance of Al-5Ti-1B master alloy on aluminium, Mat. Sci. Eng. A-Struct. 405 (1–2) (2005) 306–312.
[23] Y.L. Li, H.K. Feng, F.R. Cao, Y.B. Chen, L.Y. Gong, Effect of high density ultrasonic on the microstructure and refining property of Al-5Ti-0.25C grain refiner alloy, Mat. Sci. Eng. A-Struct. 487 (1–2) (2008) 518–523.
[24] L. Zhang, D.G. Eskin, L. Katgerman, Influence of ultrasonic melt treatment on the formation of primary intermetallics and related grain refinement in aluminum alloys, J. Mater. Sci. 46 (15) (2011) 5252–5259.
[25] H.R. Kotadia, A. Das, E. Doernberg, R. Schmid-Fetzer, A comparative study of ternary Al–Sn–Cu immiscible alloys prepared by conventional casting and casting under high-intensity ultrasonic irradiation, Mater. Chem. Phys. 131 (1) (2011) 241–249.
[26] D. Eskin, N. Alba-Baena, T. Pabel, M. da Silva, Ultrasonic degassing of aluminium alloys: basic studies and practical implementation, Mater. Sci. Technol. 31 (1) (2015) 79–84.

[27] L. Singh, B. Singh, K.K. Saxena, Manufacturing techniques for metal matrix composites (MMC): an overview, Adv. Mater. Process. Technol. 6 (2) (2020) 441–457.

[28] G. Wang, P. Croaker, M. Dargusch, D. McGuckin, D. StJohn, Simulation of convective flow and thermal conditions during ultrasonic treatment of an Al-2Cu alloy, Comp. Mater. Sci. 134 (2017) 116–125.

[29] G. Wang, M. Dargusch, M. Easton, D. StJohn, Chapter 9 - Treatment by External Fields, in: R.N. Lumley (Ed.), Fundamentals of Aluminium Metallurgy, Woodhead Publishing2018, pp. 279-332.

[30] L. Zhang, X. Li, Z. Liu, R. Li, R. Jiang, S. Guan, B. Liu, Scalable ultrasonic casting of large-scale 2219AA Al alloys: experiment and simulation, Mater. Today Commun. 27 (2021), 102329.

[31] T. Subroto, G.S.B. Lebon, D.G. Eskin, I. Skalicky, D. Roberts, I. Tzanakis, K. Pericleous, Numerical modelling and experimental validation of the effect of ultrasonic melt treatment in a direct-chill cast AA6008 alloy billet, J. Mater. Res. Technol. 12 (2021) 1582–1596.

[32] G.M. Swallowe, J.E. Field, C.S. Rees, A. Duckworth, A photographic study of the effect of ultrasound on solidification, Acta Metall. Mater. 37 (3) (1989) 961–967.

[33] D. Shu, B.D. Sun, J.W. Mi, P.S. Grant, A high-speed imaging and modeling study of dendrite fragmentation caused by ultrasonic cavitation, Metall. Mater. Trans. A 43a (10) (2012) 3755–3766.

[34] S. Wang, J. Kang, Z. Guo, T.L. Lee, X. Zhang, Q. Wang, C. Deng, J. Mi, In situ high speed imaging study and modelling of the fatigue fragmentation of dendritic structures in ultrasonic fields, Acta Mater. 165 (2019) 388–397.

[35] S. Wang, J. Kang, X. Zhang, Z. Guo, Dendrites fragmentation induced by oscillating cavitation bubbles in ultrasound field, Ultrasonics 83 (2018) 26–32.

[36] F. Wang, I. Tzanakis, D. Eskin, J. Mi, T. Connolley, In situ observation of ultrasonic cavitation-induced fragmentation of the primary crystals formed in Al alloys, Ultrason. Sonochem. 39 (2017) 66–76.

[37] A. Priyadarshi, M. Khavari, S. Bin Shahrani, T. Subroto, L.A. Yusuf, M. Conte, P. Prentice, K. Pericleous, D. Eskin, I. Tzanakis, In-situ observations and acoustic measurements upon fragmentation of free-floating intermetallics under ultrasonic cavitation in water, Ultrason. Sonochem. 80 (2021), 105820.

[38] W.W. Xu, I. Tzanakis, P. Srirangam, W.U. Mirihanage, D.G. Eskin, A.J. Bodey, P. D. Lee, Synchrotron quantification of ultrasound cavitation and bubble dynamics in Al-10Cu melts, Ultrason. Sonochem. 31 (2016) 355–361.

[39] F. Wang, D. Eskin, J.W. Mi, C.N. Wang, B. Koe, A. King, C. Reinhard, T. Connolley, A synchrotron X-radiography study of the fragmentation and refinement of primary intermetallic particles in an Al-35 Cu alloy induced by ultrasonic melt processing, Acta Mater. 141 (2017) 142–153.

[40] D.Y. Tan, T.L. Lee, J.C. Khong, T. Connolley, K. Fezzaa, J.W. Mi, High-speed synchrotron X-ray imaging studies of the ultrasound shockwave and enhanced flow during metal solidification processes, Metall. Mater. Trans. A 46a (7) (2015) 2851–2861.

[41] B. Wang, D. Tan, T.L. Lee, J.C. Khong, F. Wang, D. Eskin, T. Connolley, K. Fezzaa, J. Mi, Ultrafast synchrotron X-ray imaging studies of microstructure fragmentation in solidification under ultrasound, Acta Mater. 144 (2018) 505–515.

[42] H.J. Huang, D. Shu, J.R. Zeng, F.G. Bian, Y.A. Fu, J. Wang, B.D. Sun, In situ small angle X-ray scattering investigation of ultrasound induced nucleation in a metallic alloy melt, Scr. Mater. 106 (2015) 21–25.

[43] N. Balasubramani, D. StJohn, M. Dargusch, G. Wang, Ultrasonic processing for structure refinement: an overview of mechanisms and application of the interdependence theory, Materials (Basel) 12 (19) (2019).

[44] B. Chalmers, Nucleation Principles of Solidification John Wiley and Sons Inc., US, 1964, pp. 62-89.

[45] A. Ramirez, M. Qian, B. Davis, T. Wilks, D.H. StJohn, Potency of high-intensity ultrasonic treatment for grain refinement of magnesium alloys, Scr. Mater. 59 (1) (2008) 19–22.

[46] M. Qian, A. Ramirez, A. Das, Ultrasonic refinement of magnesium by cavitation: clarifying the role of wall crystals, J. Cryst. Growth 311 (14) (2009) 3708–3715.

[47] J.J. Sobczak, L. Drenchev, R. Asthana, Effect of pressure on solidification of metallic materials, Int. J. Cast Met. Res. 25 (1) (2012) 1–14.

[48] D.B. Spencer, R. Mehradian, M.C. Flemings, Rheological behavior of Sn-15 pct Pb in the crystallization range, in: Proceedings of the Merton C Flemings Symposium on SolidifiCation and Materials ProCessing, 2001, pp. 189–196.

[49] A. Vogel, Turbulent flow and solidification: stir-cast microstructure, Met. Sci. 12 (12) (1978) 576–578.

[50] Z. Fan, Semisolid metal processing, Int. Mater. Rev. 47 (2) (2002) 49–85.

[51] R.D. Doherty, H.I. Lee, E.A. Feest, Microstructure of stir-cast metals, Mater. Sci. Eng. 65 (1) (1984) 181–189.

[52] M.C. Flemings, Behavior of metal-alloys in the semisolid state, Metall. Trans. A 22 (5) (1991) 957–981.

[53] N. Balasubramani, Grain refinement mechanisms during ultrasonic solidification of metals, School of Mechanical and Mining Engineering, The University of Queensland, Brisbane, Australia, 2021, p. 319.

[54] N. Balasubramani, G. Wang, D.H. StJohn, M.S. Dargusch, Current understanding of the origin of equiaxed grains in pure metals during ultrasonic solidification and a comparison of grain formation processes with low frequency vibration, pulsed magnetic and electric-current pulse techniques, J. Mater. Sci. Technol. 65 (2021) 38–53.

[55] N. Balasubramani, Y. Xu, Y. Zhang, Q. Zhai, G. Wang, D. StJohn, M. Dargusch, Investigating the grain refinement mechanisms of pulsed electric current, ultrasonic and melt stirring solidification of pure aluminium, Jom-Us 73 (12) (2021) 3873–3882.

[56] N. Balasubramani, G. Wang, D.H. StJohn, M.S. Dargusch, Mechanisms of the origin of fine and non-dendritic grains at the sonotrode-liquid metal interface during ultrasonic solidification of metals, Metall. Mater. Trans. A 52 (6) (2021) 2676–2688.

[57] O. Kudryashova, M. Khmeleva, P. Danilov, V. Dammer, A. Vorozhtsov, D. Eskin, Optimizing the conditions of metal solidification with vibration, Metals 9 (3) (2019) 366.

[58] Y. Yoshitake, K. Yamamoto, N. Sasaguri, H. Era, Grain refinement of Al–2%Cu alloy using vibrating mold, Int. J. Metalcast. 13 (3) (2019) 553–560.

[59] H.M. Guo, A.S. Zhang, X.J. Yang, M.M. Yan, Y. Ding, Microstructure formation and mechanical properties of AZ31 magnesium alloy solidified with a novel mechanical vibration technique, Metall. Mater. Trans. A 45a (1) (2014) 438–446.

[60] R.-G. Guan, D. Tie, A review on grain refinement of aluminum alloys: progresses, challenges and prospects, Acta Metall. Sinica (English Letters) 30 (5) (2017) 409–432.

[61] K.A. Ramisetty, A.B. Pandit, P.R. Gogate, Investigations into ultrasound induced atomization, Ultrason. Sonochem. 20 (1) (2013) 254–264.

[62] B. Avvaru, M.N. Patil, P.R. Gogate, A.B. Pandit, Ultrasonic atomization: effect of liquid phase properties, Ultrasonics 44 (2) (2006) 146–158.

[63] R. Rajan, A.B. Pandit, Correlations to predict droplet size in ultrasonic atomisation, Ultrasonics 39 (4) (2001) 235–255.

[64] S. Wisutmethangoon, T. Plookphol, P. Sungkhaphaitoon, Production of SAC305 powder by ultrasonic atomization, Powder Technol. 209 (1) (2011) 105–111.

[65] E.G. Lierke, G. Grießhammer, The formation of metal powders by ultrasonic atomization of molten metals, Ultrasonics 5 (4) (1967) 224–228.

[66] N. Balasubramani, N. Yang, J. Venezuela, M. Dargusch, Ultrasonic treatment for the refinement of brittle CaZn13 phases in a biomedical Zn-Cu-Ca alloy, Mater. Lett. 305 (2021), 130754.

[67] Z. Liu, R. Li, R. Jiang, L. Zhang, X. Li, Scalable ultrasound-assisted casting of ultra-large 2219 Al alloy ingots, Metall. Mater. Trans. A 50 (3) (2019) 1146–1152.

[68] J. Hutt, D. StJohn, The origins of the equiaxed zone—Review of theoretical and experimental work, Int. J. Cast Met. Res. 11 (1) (1998) 13–22.

[69] A. Ohno, Controlling the Macro Structure of Cast Metals, Solidification: The Separation Theory and its Practical Applications, Springer Berlin Heidelberg, Berlin, Heidelberg, 1987, pp. 42–82.

[70] T. Motegi, A. Ohno, Origin of showering crystals in the molten metal in a mold cooled from the top, J. Jpn. Inst. Met. 44 (4) (1980) 359–366.

[71] Y.C. Lee, A.K. Dahle, D.H. StJohn, The role of solute in grain refinement of magnesium, Metall. Mater. Trans. A 31 (11) (2000) 2895–2906.

[72] B. Nagasivamuni, G. Wang, D.H. StJohn, M.S. Dargusch, Effect of ultrasonic treatment on the alloying and grain refinement efficiency of a Mg – Zr master alloy added to magnesium at hypo- and hyper-peritectic compositions, J. Cryst. Growth 512 (2019) 20–32.

[73] S. Chankitmunkong, D.G. Eskin, C. Limmaneevichitr, Structure refinement, mechanical properties and feasibility of deformation of hypereutectic Al–Fe–Zr and Al–Ni–Zr alloys subjected to ultrasonic melt processing, Mater. Sci. Eng., A 788 (2020), 139567.

[74] H. Huang, L. Qin, H. Tang, D. Shu, W. Yan, B. Sun, J. Mi, Ultrasound cavitation induced nucleation in metal solidification: an analytical model and validation by real-time experiments, Ultrason. Sonochem. 80 (2021), 105832.

[75] X. Zhang, H.R. Kotadia, J. Depner, M. Qian, A. Das, Effect of Ultrasonication on the Solidification Microstructure in Al and Mg-Alloys, in: C. Chesonis (Ed.), Light Metals 2019, Springer International Publishing, Cham, 2019, pp. 1589–1595.

[76] N. Srivastava, G.P. Chaudhari, Grain refinement in ultrasonicated binary aluminium alloys, J. Cryst. Growth 532 (2020), 125415.

[77] G. Wang, Q. Wang, N. Balasubramani, M. Qian, D.G. Eskin, M.S. Dargusch, D. H. StJohn, The role of ultrasonically induced acoustic streaming in developing fine equiaxed grains during the solidification of an Al-2 Pct Cu alloy, Metall. Mater. Trans. A 50 (11) (2019) 5253–5263.

[78] B. Nagasivamuni, G. Wang, D.H. StJohn, M.S. Dargusch, Mechanisms of Grain Formation During Ultrasonic Solidification of Commercial Purity Magnesium, Springer International Publishing, Cham, 2019, pp. 1579–1586.

[79] N. Balasubramani, G. Wang, M.A. Easton, D.H. StJohn, M.S. Dargusch, A comparative study of the role of solute, potent particles and ultrasonic treatment during solidification of pure Mg, Mg–Zn and Mg–Zr alloys, J. Magnes. Alloy 9 (3) (2021) 829–839.

[80] N. Balasubramani, G. Wang, D.H. StJohn, M.S. Dargusch, The poisoning effect of Al and Be on Mg—1 wt.% Zr alloy and the role of ultrasonic treatment on grain refinement, Front. Mater. 6 (322) (2019).

[81] B. Nagasivamuni, G. Wang, D.H. StJohn, M.S. Dargusch, The effect of ultrasonic treatment on the mechanisms of grain formation in as-cast high purity zinc, J. Cryst. Growth 495 (2018) 20–28.

[82] N. Yang, N. Balasubramani, J. Venezuela, S. Almathami, C. Wen, M. Dargusch, The influence of Ca and Cu additions on the microstructure, mechanical and degradation properties of Zn–Ca–Cu alloys for absorbable wound closure device applications, Bioact. Mater. 6 (5) (2021) 1436–1451.

[83] A. Pola, M. Tocci, F.E. Goodwin, Review of microstructures and properties of zinc alloys, Metals 10 (2) (2020) 253.

[84] A.S.M.I.H. Committee, 21.1.2 Zinc Alloy Castings, ASM Handbook, Volume 02 - Properties and Selection: Nonferrous Alloys and Special-Purpose Materials, ASM International 1990.

[85] S.W.K. Morgan, Zinc and Its Alloys and Compounds, John Wiley and Sons, New York, 1985.

[86] R.J. Barnhurst, Zinc and Zinc Alloys, in: A.S.M.H. Committee (Ed.), Properties and Selection: Nonferrous Alloys and Special-Purpose Materials, ASM International, 1990.

[87] P. Chollet, Recent progress in the metallurgy of wrought-zinc alloys, Can. Metall. Q. 7 (3) (1968) 177–185.
[88] Z. Liu, D. Qiu, F. Wang, J.A. Taylor, M. Zhang, Grain refinement of cast zinc through magnesium inoculation: Characterisation and mechanism, Mater Charact 106(Supplement C) (2015) 1-10.
[89] Z. Liu, D. Qiu, F. Wang, J.A. Taylor, M. Zhang, The grain refining mechanism of cast zinc through silver inoculation, Acta Mater. 79 (2014) 315–326.
[90] Z.L. Liu, F. Wang, D. Qiu, J.A. Taylor, M.X. Zhang, The effect of solute elements on the grain refinement of cast Zn, Metall. Mater. Trans. A 44a(9) (2013) 4025-4030.
[91] Z.L. Liu, D. Qiu, F. Wang, J.A. Taylor, M.X. Zhang, Effect of grain refinement on tensile properties of cast zinc alloys, Metall. Mater. Trans. A 47a (2) (2016) 830–841.
[92] H. Kabir, K. Munir, C. Wen, Y. Li, Recent research and progress of biodegradable zinc alloys and composites for biomedical applications: biomechanical and biocorrosion perspectives, Bioact. Mater. 6 (3) (2021) 836–879.
[93] N. Yang, J. Venezuela, S. Almathami, M. Dargusch, Zinc-nutrient element based alloys for absorbable wound closure devices fabrication: current status, challenges, and future prospects, Biomaterials 280 (2022), 121301.
[94] J. Venezuela, M.S. Dargusch, The influence of alloying and fabrication techniques on the mechanical properties, biodegradability and biocompatibility of zinc: a comprehensive review, Acta Biomater. 87 (2019) 1–40.
[95] H.F. Li, Z.Z. Shi, L.N. Wang, Opportunities and challenges of biodegradable Zn-based alloys, J. Mater. Sci. Technol. 46 (2020) 136–138.
[96] H.N. Kim, K.S. Suslick, The effects of ultrasound on crystals: sonocrystallization and sonofragmentation, Crystals 8 (7) (2018) 280.
[97] R. Prasad, S.V. Dalvi, Sonocrystallization: monitoring and controlling crystallization using ultrasound, Chem. Eng. Sci. 226 (2020), 115911.
[98] J.R.G. Sander, B.W. Zeiger, K.S. Suslick, Sonocrystallization and sonofragmentation, Ultrason. Sonochem. 21 (6) (2014) 1908–1915.
[99] M.D. Luque de Castro, F. Priego-Capote, Ultrasound-assisted crystallization (sonocrystallization), Ultrason. Sonochem. 14 (6) (2007) 717–724.
[100] H.R. Kotadia, M. Qian, D.G. Eskin, A. Das, On the microstructural refinement in commercial purity Al and Al-10wt% Cu alloy under ultrasonication during solidification, Mater. Des. 132 (2017) 266–274.
[101] S. Ji, Z. Fan, Solidification behavior of Sn-15 wt pct Pb alloy under a high shear rate and high intensity of turbulence during semisolid processing, Metall. Mater. Trans. A 33 (11) (2002) 3511–3520.
[102] W.L. Wang, K.S. Wang, X. Lin, In situ nucleation and detachment of dendrites to form equiaxed grains stirred by vibration, Int. J. Cast Met. Res. 23 (1) (2010) 65–68.
[103] H.R. Kotadia, A. Das, Modification of solidification microstructure in hypo- and hyper-eutectic Al–Si alloys under high-intensity ultrasonic irradiation, J. Alloy. Compd. 620 (2015) 1–4.
[104] S.-B. Kim, Y.-H. Cho, J.-G. Jung, W.-H. Yoon, Y.-K. Lee, J.-M. Lee, Microstructure-strengthening interrelationship of an ultrasonically treated hypereutectic Al–Si (A390) alloy, Met. Mater. Int. 24 (6) (2018) 1376–1385.
[105] J. Sun, T. Yamamoto, S. Komarov, Behavior of Al-Zr intermetallic compound particles under high-amplitude ultrasound irradiation into molten aluminum, J. Alloy. Compd. 912 (2022), 165128.
[106] F. Wang, D. Eskin, T. Connolley, J. Mi, Effect of ultrasonic melt treatment on the refinement of primary Al3Ti intermetallic in an Al–0.4Ti alloy, J. Cryst. Growth 435 (2016) 24–30.
[107] T.V. Atamanenko, D.G. Eskin, M. Sluiter, L. Katgerman, On the mechanism of grain refinement in Al–Zr–Ti alloys, J. Alloy. Compd. 509 (1) (2011) 57–60.
[108] H.R. Kotadia, M. Qian, A. Das, Microstructural modification of recycled aluminium alloys by high-intensity ultrasonication: observations from custom Al–2Si–2Mg–1.2Fe–(0.5,1.0)Mn alloys, J. Alloy. Compd. 823 (2020), 153833.
[109] C. Wang, T. Connolley, I. Tzanakis, D. Eskin, J. Mi, Characterization of ultrasonic bubble clouds in a liquid metal by synchrotron X-ray high speed imaging and statistical analysis, Materials 13 (1) (2020) 44.
[110] G.S.B. Lebon, G. Salloum-Abou-Jaoude, D. Eskin, I. Tzanakis, K. Pericleous, P. Jarry, Numerical modelling of acoustic streaming during the ultrasonic melt treatment of direct-chill (DC) casting, Ultrason. Sonochem. 54 (2019) 171–182.
[111] Y. Zuo, J. Cui, Z. Zhao, H. Zhang, L. Li, Q. Zhu, Mechanism of grain refinement of an Al–Zn–Mg–Cu alloy prepared by low-frequency electromagnetic casting, J. Mater. Sci. 47 (14) (2012) 5501–5508.